CANCER

Anti-seed PNAs targeting multiple oncomiRs for brain tumor therapy

Yazhe Wang[1]†, Shipra Malik[2]†, Hee-Won Suh[1], Yong Xiao[1], Yanxiang Deng[1], Rong Fan[1], Anita Huttner[3], Ranjit S. Bindra[4], Vijender Singh[5], W. Mark Saltzman[1]*, Raman Bahal[2]*

Glioblastoma (GBM) is one of the most lethal malignancies with poor survival and high recurrence rates. Here, we aimed to simultaneously target oncomiRs 10b and 21, reported to drive GBM progression and invasiveness. We designed short (8-mer) γ-modified peptide nucleic acids (sγPNAs), targeting the seed region of oncomiRs 10b and 21. We entrapped these anti-miR sγPNAs in nanoparticles (NPs) formed from a block copolymer of poly(lactic acid) and hyperbranched polyglycerol (PLA-HPG). The surface of the NPs was functionalized with aldehydes to produce bioadhesive NPs (BNPs) with superior transfection efficiency and tropism for tumor cells. When combined with temozolomide, sγPNA BNPs administered via convection-enhanced delivery (CED) markedly increased the survival (>120 days) of two orthotopic (intracranial) mouse models of GBM. Hence, we established that BNPs loaded with anti-seed sγPNAs targeting multiple oncomiRs are a promising approach to improve the treatment of GBM, with a potential to personalize treatment based on tumor-specific oncomiRs.

INTRODUCTION

Brain and nervous system cancers are projected to account for 1.3% of cancer cases and ~3% of cancer deaths in 2022 (1). Glioblastoma (GBM) accounts for about 14.5% of nervous system tumors, with a median survival of only 15 months (2). In the United States, GBM has an incidence rate of 4.32 per 100,000 person-years (3) and a 1-year survival rate of only 1.4% in patients over 75 years of age (4). The primary therapeutic approach for GBM is surgical resection followed by radiotherapy and chemotherapy. Temozolomide (TMZ) improves the 2-year survival rate from 10.4 to 26.5% in combination with radiotherapy, compared to radiotherapy alone (5). Hence, there is a need for improved therapeutic approaches for targeting molecular genetic mediators of GBM.

MicroRNAs (miRNAs or miRs) are ~20- to 25-nucleotide long noncoding RNAs that regulate gene expression at the posttranscriptional level (6). The dysregulation of miRs, either up-regulation (where they are known as oncomiRs) or down-regulation, plays an important role in several malignancies (7). Previous studies have reported aberrant miR expression levels in patients with GBM; some of these are associated with poor prognosis and low overall survival (8). In particular, miR-10b (9, 10) and miR-21 (11, 12) appear to be the most highly up-regulated oncomiRs contributing to GBM. miR-10b enhances GBM growth by negatively regulating BCL2 interacting mediator of death (Bim), transcription factor AP-2γ (TFAP2C), tumor suppressor cyclin-dependent kinase 2A inhibitor (CDKN2A/16), and cyclin-dependent kinase inhibitor I (p21) expression (10). Inhibiting miR-10b reduces the growth of intracranial GBM tumors in animal models (13, 14). These promising results have prompted the development of an investigational

antisense oligonucleotide targeting miR-10b (RGLS5799, Regulus Therapeutics). Similarly, up-regulated miR-21 levels increase GBM invasiveness by inhibiting matrix metalloproteinase (MMP) (11), inducing proliferation via negative regulation of insulin-like growth factor–binding protein-3 (IGFBP3) (12) or phosphatase and tensin homolog (PTEN), and promoting tumor stemness via SRY-box transcription factor-2 (SOX-2) (15, 16). Hence, knocking down miR-21 reduces GBM progression and invasion (17, 18) in addition to preventing chemoresistance of GBM cells to TMZ (19) and Taxol (20). Current therapeutic strategies, which are focused on targeting a single oncomiR, have shown limited efficacy against GBM. Few studies have reported that inhibition of oncomiRs 10b and 21 induces apoptosis and sensitizes glioma cells to TMZ both in vitro (21, 22) and, to some extent, in vivo (23).

In this study, we aimed at targeting miR-10b and miR-21 simultaneously to extend the survival and enhance the chemosensitization of GBM toward TMZ. Peptide nucleic acids (PNAs) are synthetic nucleic acid analogs where the phosphodiester backbone is substituted with neutral N-(2-aminoethyl) glycine units (24). PNAs bind to target miRs via complementary Watson and Crick base pairing, but they are enzymatically stable (25, 26). Classical PNAs targeting full-length oncomiRs have been explored for cancer therapy (27, 28), but the functional activity of miRs is governed by the "seed region" centered on nucleotides 2 to 7 on the 5′ end (29). Hence, anti-miR efficacy can be achieved by targeting only the seed region of the oncomiRs (30). Here, we designed serine–gamma PNAs (γPNAs) complementary to the seed region of oncomiR-21 and oncomiR-10b to achieve improved anti-miR activity. Because PNAs with certain modifications at the γ position (γPNAs) are preorganized into a helical conformation due to the presence of chirality at the γ position, they have superior physicochemical features, binding affinity, and specificity compared to classical PNAs (31), making it possible to target short sequences with high affinity. Short anti-seed γPNAs (sγPNAs) have numerous appealing features: Synthesis is straightforward; quality control analysis is simplified over longer sequences, and they are well suited for conjugation with fluorophores or other entities to enable imaging.

[1]Department of Biomedical Engineering, Yale University, New Haven, CT 06511, USA. [2]Department of Pharmaceutical Sciences, University of Connecticut, Storrs, CT 06269, USA. [3]Department of Pathology, Yale University, New Haven, CT 06510, USA. [4]Department of Therapeutic Radiology, Yale University, New Haven, CT 06510, USA. [5]Computational Biology Core, Institute for Systems Genomics, University of Connecticut, Storrs, CT 06269, USA.
*Corresponding author. Email: raman.bahal@uconn.edu (R.B.); mark.saltzman@yale.edu (W.M.S.)
†These authors contributed equally to this work.

Anti-seed syPNAs are clinically more translatable and have comparable in vivo efficacy to conventional full-length anti-miRs with minimal toxicity (30, 32, 33).

Over the past years, we have developed an approach for the delivery of agents directly to brain tumors, using convection-enhanced delivery (CED) to introduce polymeric nanoparticles (NPs) that are loaded with active agents, directly into the brain (34). NPs are composed of a block copolymer of poly(lactic acid) and hyperbranched polyglycerol (PLA-HPG), which can be surface-functionalized to introduce aldehyde (CHO) groups (35), creating PLA-HPG-CHO that confers several advantages for the delivery of PNA anti-miRs. NPs formed from PLA-HPG-CHO are bioadhesive NPs (BNPs) (36, 37). We have shown that, compared with several other NPs of similar composition, these BNPs lead to the highest level of uptake into intracranial tumor cells after CED (38), and they can be loaded with PNAs, which are slowly released in the brain after CED (18). In this work, we loaded the PLA-HPG-CHO BNPs with two syPNAs, one binding to miR-10b and another binding to miR-21, to test the hypothesis that simultaneous delivery of two anti-miRs in glioma cells can regulate unique molecular pathways leading to improved survival.

RESULTS

Design and synthesis of PNA oligomers

Regular and serine-γPNA oligomers targeting oncomiR-21 and oncomiR-10b were synthesized on a solid support using standard butoxycarbonyl (Boc) chemistry protocols (Fig. 1, A to C) (39). syPNA-21 and syPNA-10b are syPNAs, with a serine modification at the γ position, designed to bind the seed region of oncomiRs 21 and 10b, respectively. Furthermore, syPNA-21 and syPNA-10b were extended with three arginine residues on the N terminus to increase the binding to their respective targets via electrostatic

interaction between the cationic domain of γPNAs and the negatively charged backbone in the flanking region of miR (40). Scrambled versions of these PNAs, Scr-syPNA-21 and Scr-syPNA-10b, were used as controls. To compare the efficacy of short cationic γPNAs with full-length regular PNAs, we also synthesized PNA-21 and PNA-10b, which were designed to target full-length oncomiRs 21 and 10b, respectively (Fig. 1C). TAMRA dye (5-carboxytetramethylrhodamine) was conjugated to the N terminus of the PNAs for visualization of cellular uptake and biodistribution. Reversed-phase high-performance liquid chromatography (RP-HPLC) and mass spectrometry analyses confirmed the high quality of the synthesized PNAs (fig. S1 and table S1).

syPNAs bind to the target oncomiRs with high affinity and specificity

Binding affinity was measured by incubating the PNAs with the target oncomiRs. syPNA-21 and syPNA-10b were incubated with miR-21 and miR-10b, respectively, under simulated physiological conditions at two different ratios of 2:1 and 4:1 (PNA:miR) for 16 hours. Both syPNA-21 and syPNA-10b showed substantial binding to their respective targets even at the lower 2:1 ratio (fig. S2A), as evidenced by the faint band corresponding to the unbound miRs and the prominent retarded band of the PNA-miR heteroduplexes. The band for target miR-21 and miR-10b completely disappeared on incubation with their respective PNAs at a 4:1 ratio (fig. S2B). We also studied the binding of syPNA-21 and syPNA-10b in the presence of both miR-10b and miR-21. When incubated with the target miR-21 at a 1:1 ratio, syPNA-21 showed a retarded band (fig. S3, lane 3). As expected, on incubation of syPNA-21 with miR-10b, we did not observe any shift in the band (fig. S3, lane 6). Incubation of syPNA-21 with both the miRs resulted in only one retarded band (fig. S3, lane 7), similar to the syPNA-21-miR-21 heteroduplex, indicating the specificity of syPNA-21 toward the target miR-21. Similarly, syPNA-10b showed a shifted band only after incubation with the target miR-10b (fig. S3, lane 4), and no retarded band was visible in the presence of miR-21 (fig. S3, lane 5). Furthermore, on incubation with both the miRs, syPNA-10b showed one retarded band similar to the syPNA-10b-miR-10b heteroduplex. Hence, syPNA-21 and syPNA-10b showed high binding affinity and specificity toward miR-21 and miR-10b, respectively.

Preparation and characterization of NPs

PNAs were encapsulated in PLA-HPG to produce nonadhesive NPs (NNPs) using a modified single-emulsion method as previously reported (18, 35). BNPs were prepared by brief exposure of these NNPs to sodium periodate, converting the vicinal diols of HPG to aldehydes, creating HPG-CHO; successful conversion to the bioadhesive state was confirmed by measuring BNP adhesion to a poly(L-lysine)–coated glass (fig. S4). For the simultaneous knockdown of target oncomiRs 10b and 21, different batches of NPs formulated with respective PNAs were physically mixed at a fixed PNA molar ratio (1:1) (Fig. 1D). Single syPNA-loaded NPs and combinations of NP formulations (syPNA/NNP:syPNA/PLA-HPG and syPNA/BNP:γPNA/PLA-HPG-CHO) were extensively characterized (Table 1). syPNA/NNP and syPNA/BNP had similar average hydrodynamic sizes, ranging from 150 to 165 nm, as measured by dynamic light scattering (DLS). All the NP formulations exhibited negative surface charge in water with ζ potential between −20 and

Table 1. Hydrodynamic diameter, ζ potential, and PNA loading in NPs. The data are shown as means ± SD ($n = 3$). Scr-syPNA/NNP was the physical mixture of Scr-syPNA-21–loaded NNP and Scr-syPNA-10b–loaded NNP, syPNA/BNP was the mixture of syPNA-21–loaded BNP and syPNA-10b–loaded BNP, and PNA/BNP was the mixture of PNA-21–loaded BNP and PNA-10b–loaded BNP. NNP indicates PLA-HPG NP, and BNP indicates PLA-HPG-CHO NP.

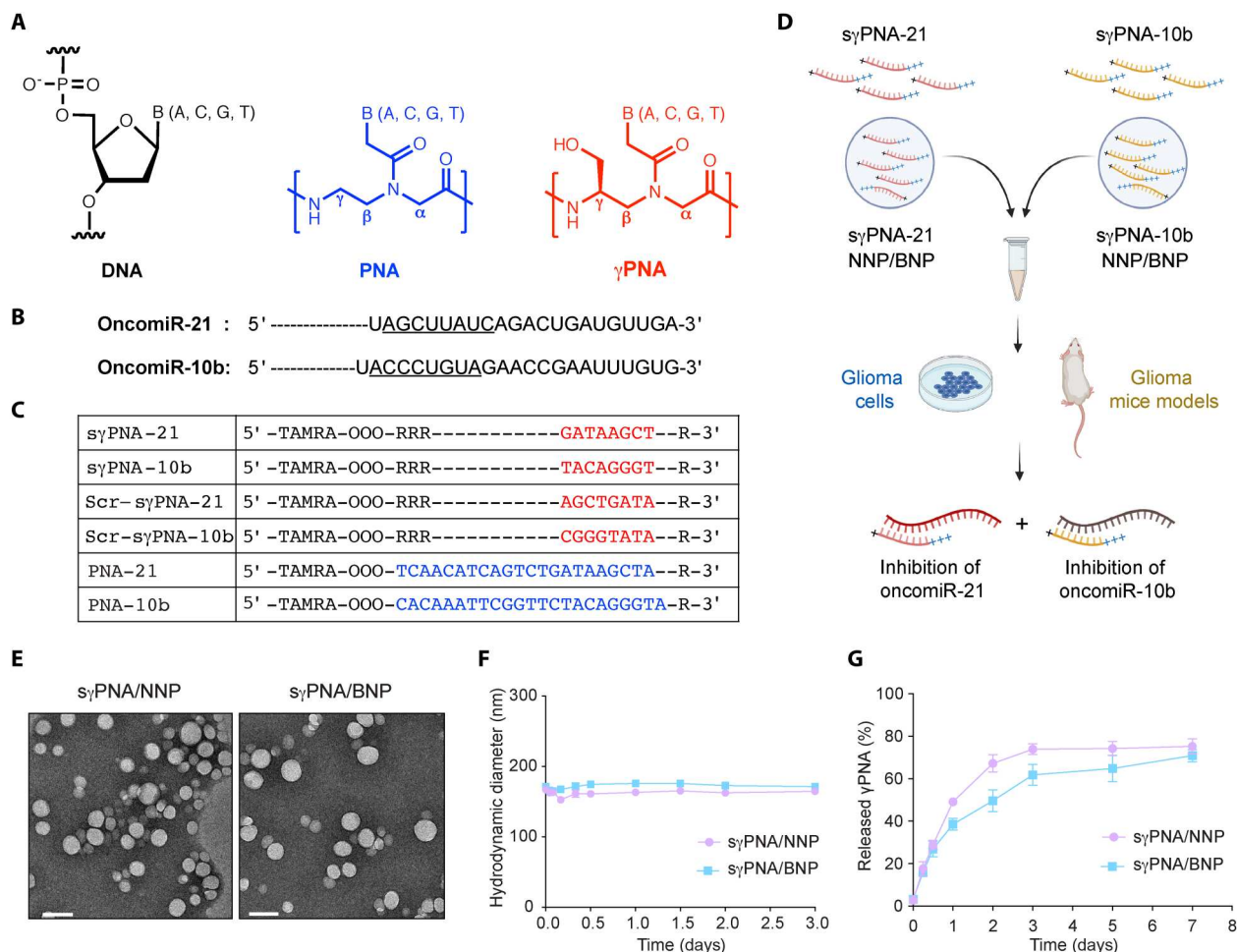| Formulation	Hydrodynamic diameter (nm)	ζ potential (mV)	PNA loading (nmol/mg)
syPNA-21/NNP	160 ± 4	−21 ± 3	1.5 ± 0.2
syPNA-21/BNP	170 ± 4	−30 ± 4	1.5 ± 0.4
syPNA-10b/NNP	150 ± 6	−21 ± 5	1.6 ± 0.3
syPNA-10b/BNP	160 ± 5	−32 ± 3	1.4 ± 0.3
Scr-syPNA/NNP	180 ± 6	−22 ± 2	1.4 ± 0.2
syPNA/BNP	170 ± 3	−32 ± 3	1.5 ± 0.3
PNA/BNP	170 ± 6	−28 ± 2	1.9 ± 0.2

Fig. 1. Design of PNAs and characterization of NPs. (**A**) Chemical structure of DNA, PNA, and serine-γ-PNA. (**B**) The sequence of oncomiR-21 and oncomiR-10b, where the underlined segment is the seed region. (**C**) PNAs used in the study. sγPNA-21 and sγPNA-10b are serine-γPNAs designed to bind the seed region of oncomiR-21 and oncomiR-10b, respectively. Three arginine (RRR) residues are appended to the N terminus and one arginine (R) on the C terminus. Scr-sγPNA-21 and Scr-sγPNA-10b are scrambled versions of sγPNA-21 and sγPNA-10b, respectively. PNA-21 and PNA-10b are regular PNAs designed to bind full-length oncomiR-21 and oncomiR-10b, respectively. PNAs were conjugated with TAMRA, a fluorescent dye for imaging. OOO represents 8-amino-2,6,10-trioxaoctanoic acid residues (Mini-PEG). (**D**) Graphical representation of sγPNA encapsulation in NPs (NNP or BNP) and treatment strategy for the simultaneous inhibition of oncomiRs 21 and 10b. (**E**) TEM images of sγPNA/NNP and sγPNA/BNP. Scale bars, 100 nm. (**F**) Size stability of sγPNA/NNP and sγPNA/BNP in aCSF. (**G**) The amount of sγPNA (sγPNA-21 and sγPNA-10b) released from NPs over time during incubation in buffered saline was determined and quantified as a percentage of the amount loaded. The data are shown as means ± SD (n = 3).

−30 mV. The average PNA loading was around 1.5 nmol/mg of NPs, suggesting superior encapsulation efficiency. Transmission electron microscopy (TEM) images showed uniform and spherical morphology of sγPNA/BNP and sγPNA/NNP (Fig. 1E). The majority of visible NPs were around 100 nm in diameter, which confirmed the desired particle size. Both sγPNA/NNP and sγPNA/BNP were stable with no measurable aggregation during 3 days of incubation in artificial cerebrospinal fluid (aCSF) (Fig. 1F). In vitro sγPNAs′ release from both NNP and BNP during continuous incubation in phosphate-buffered saline (PBS) at 37°C was similar (Fig. 1G), with slightly slower release from BNPs.

sγPNA-loaded BNPs show superior cellular uptake in glioma cells

TAMRA fluorescence from sγPNAs was used to quantify the uptake of NPs in glioma cells. From microscopic observation, cells treated with either NNP or BNP showed stronger TAMRA fluorescence than cells treated with free sγPNA. Confocal microscopy (Fig. 2, A and B) indicated that treatment with BNP led to higher cellular uptake than with NNP in U87 cells and G22 cells from a patient-derived xenograft (PDX); BNP also produced wider distribution throughout the cells. Flow cytometry analysis revealed that the uptake of BNP was higher than that of NNP (Fig. 2, C and D) in both cell types. Free sγPNAs showed no uptake after 24 hours of incubation. Similar results were obtained in a different human glioma cell line, LN229 (fig. S5). In a recent study, we found that both NNP and BNP undergo cellular uptake via endocytosis in tumor cells. Mechanistic investigations showed that NNPs use both macropinocytosis and clathrin-mediated pathways, whereas BNPs are internalized via clathrin-mediated endocytosis (*41*). Furthermore, lysosome staining of treated U87 cells showed colocalization of both NNP and BNP in lysosomes at 4 hours (fig. S6). After
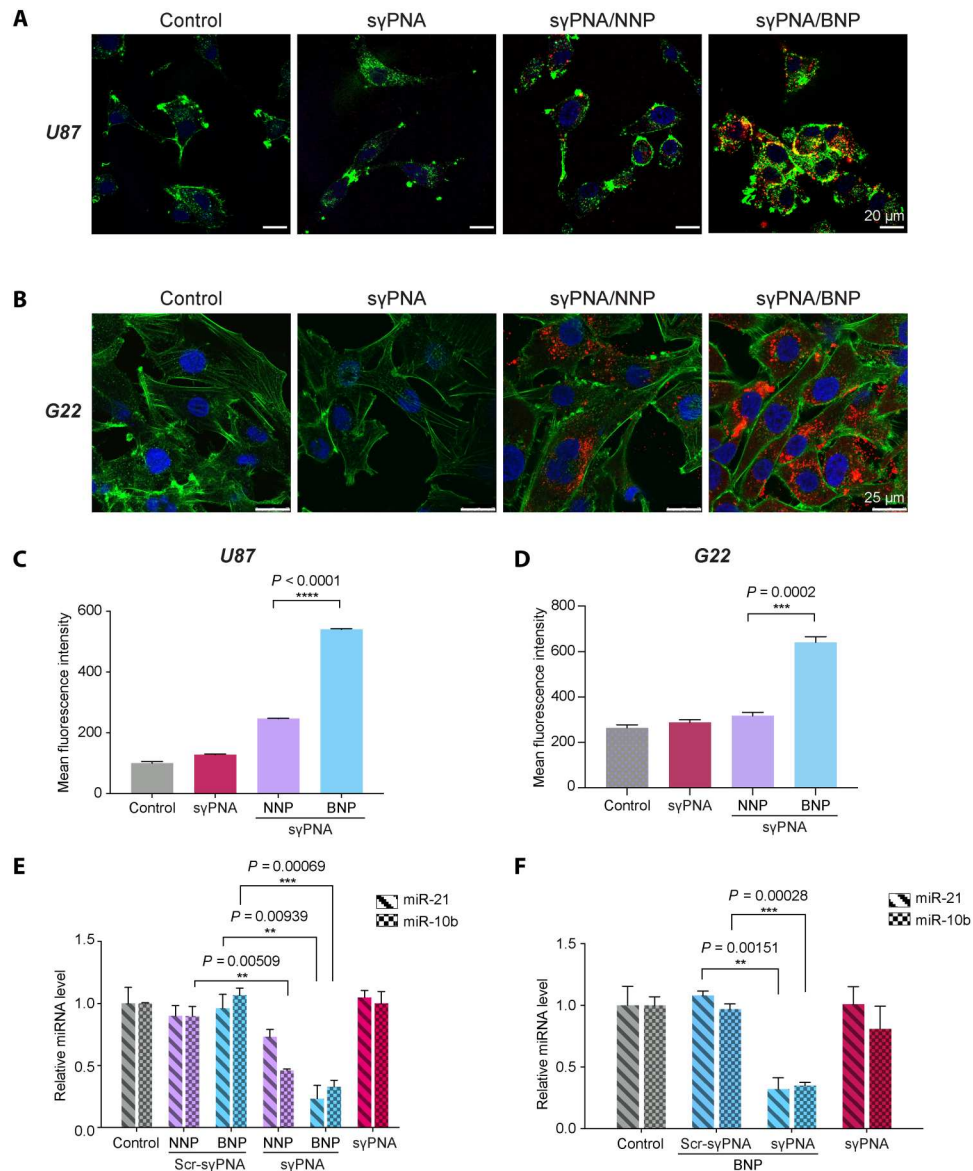
Fig. 2. sγPNA-mediated simultaneous knockdown of miR-21 and miR-10b in multiple glioma cells. (**A**) Confocal microscopic image of U87 cells treated with free sγPNA or sγPNA-loaded NPs. Scale bars, 20 μm. (**B**) Confocal microscopic images of G22 cells (patient-derived GBM cells) treated with free sγPNA or sγPNA-loaded NPs. Scale bars, 25 μm. PNAs were conjugated with TAMRA (red); F-actin was labeled with phalloidin (green), and the nucleus was stained with Hoechst (blue). (**C**) Cellular uptake in U87 cells analyzed by flow cytometry. Data are expressed as means ± SD (*n* = 3). (**D**) Quantification of cellular uptake of sγPNA in G22 cells via flow cytometry analysis. Data are expressed as means ± SD (*n* = 3). (**E**) Expression analysis of miR-10b and miR-21 levels in U87 cells after treatment with Scr-sγPNA/NNP, Scr-sγPNA/BNP, sγPNA/NNP, sγPNA/BNP, and free sγPNA. (**F**) The levels of miR-10b and miR-21 in G22 cells treated in vitro with sγPNAs (sγPNA-10b + sγPNA-21) and BNPs containing sγPNAs and scr-sγPNAs. sγPNA/BNPs are a physical mixture of sγPNA-21 BNP and sγPNA-10b BNP. sγPNA/NNPs are a physical mixture of sγPNA-21 NNP and sγPNA-10b NNP. NNP indicates PLA-HPG NP, and BNP indicates PLA-HPG-CHO NP.

24 hours of treatment, an increased fluorescent signal of PNA was found in the cytoplasm, particularly in BNP-exposed cells; a lower level of colocalization with lysosomes was also noticed with broadly distributed red fluorescence from PNA. These findings confirm the preferential cellular uptake of sγPNA/BNP into glioma cells, which is consistent with our previous studies (*18*, *38*).

sγPNA-loaded BNPs inhibit the expression of miR-10b and miR-21

To confirm the therapeutic efficacy of designed anti-miR sγPNAs, different types of PNA-loaded NP formulations or free sγPNAs were incubated with U87 and G22 (PDX) cells. Cellular levels of miR-21 and miR-10b were substantially reduced 72 hours after treatment with NPs (Fig. 2, E and F). In both U87 and G22 cells, a notable decrease in miR-10b and miR-21 expression was achieved following incubation with sγPNA/BNP when compared to the

control treatment. Scrambled versions of sγPNA NP formulations and free sγPNAs had no effect on miR-10b and miR-21 expression. sγPNA/NNP produced a notable decrease in miR-10b expression but not a statistically significant effect on miR-21 expression in U87 cells, suggesting insufficient knockdown (Fig. 2E). Notably, sγPNA/BNP showed greater suppression of both oncomiRs than full-length PNA-loaded NPs (PNA/BNP), which we believe reflects the higher binding affinity of sγPNAs (fig. S7A). We found that *PTEN*, one of the most frequently mutated tumor suppressor genes in human cancer (*42*) and a predicted target of both miR-21 (*43*) and miR-10b (*13*), was up-regulated by four- to five-fold after treatment with sγPNA-loaded NPs (fig. S7B). Moreover, the specific inhibition of miR-21 mediated by sγPNA-21–loaded NPs did not affect the expression of miR-10b, and, likewise, sγPNA-10b–loaded NPs did not affect the expression of miR-21 (fig. S7C). These results demonstrated the specific and effective knockdown of target oncomiRs provided by sγPNA-loaded NPs, with BNPs providing the strongest biological effect.

sγPNA-loaded BNPs induce enhanced apoptosis in combination with TMZ

Apoptosis was measured by annexin V and propidium iodide (PI) staining in U87 (fig. S8) and G22 cells after treatment with sγPNA-loaded NPs. Apoptosis was enhanced by sγPNA/BNP treatment (compared to sγPNA/NNP-treated or control cells). Furthermore, the combination of sγPNA/BNP with TMZ showed a higher apoptotic population in comparison to the only TMZ- or sγPNA/BNP-treated cells (Fig. 3, A and B). Cotreatment with TMZ and sγPNA/BNP led to higher apoptotic activity than with full-length PNA BNP (fig. S9A). Caspase 3 and caspase 7 activities, key indicators of apoptosis, were elevated two-fold after TMZ and sγPNA/BNP cotreatment (fig. S9, B and C).

Tumor cell death by combination treatment with TMZ

Recent studies show that miRs play a role in TMZ resistance and that regulation of miR can enhance TMZ-induced cell death (*44*). To assess the activity to induce tumor cell death, we tested sγPNA-loaded BNP and TMZ on a series of GBM cell lines including PDX cells G22, GBM-derived stem cells PS30, human GBM cells U87 and LN229, TMZ-resistant LN229 (LN229-TR), and mouse glioma cells SB28 (Fig. 3, C to H). We found that the treatment of GBM cells with sγPNA-loaded BNPs sensitized the cells to TMZ compared with scrambled sγPNA-loaded BNPs. The half-inhibitory concentration (IC_{50}) showed a remarkable decrease in cell viability of the six tested GBM cells treated by sγPNA/BNP and TMZ (Fig. 3I), indicating robust antitumor activity of this combined treatment. Both sγPNA/NNP and sγPNA/BNP showed dose-dependent cytotoxicity against U87 cells (fig. S10A). sγPNA/BNP displayed higher cell killing activity and resulted in up to 54% of cell death after treatment for 72 hours, while sγPNA/NNP induced 43% of cell death under the same condition. The oncogenic miR-targeting combination treatment with or without NPs did not produce any toxicity on human astrocytes (fig. S10, B and C).

Simultaneous inhibition of miR-10b and miR-21 affects phosphatidylinositol 3-kinase–Akt, focal adhesion, and hypoxia-inducible factor-1 pathways

To identify the cellular pathways associated with the inhibition of tumor growth, we performed RNA sequencing (RNA-seq) in

sγPNA/BNP-treated U87 cells (fig. S11). Up-regulated and down-regulated genes were identified in treated U87 cells in comparison to the control using a 1.5-fold change cutoff value with a significance [adjust P (P_{adj})] value of <0.05 (fig. S12). The hierarchical clustering of log-transformed fold change values of differentially and significantly expressed genes (Fig. 4A) revealed a substantial number of dysregulated genes after the knockdown of oncomiRs 21 and 10b in comparison to the knockdown of an individual oncomiR (figs. S13 and S14). Gene ontology analysis in U87 cells after the knockdown of miR-21 indicated the enrichment of differentially expressed genes (DEGs) associated with PI3K-Akt (phosphatidylinositol 3-kinase/Akt) and focal adhesion pathways (fig. S15), while miR-10b knockdown resulted in the enrichment of only PI3K-Akt pathway (fig. S16). However, we observed a substantial enrichment of down-regulated DEGs in three major cancer-associated pathways—PI3K-Akt, HIF-1 (hypoxia-inducible factor-1), and focal adhesion—involved in angiogenesis, proliferation, survival, and metastasis of tumor cells (Fig. 4B) after knockdown of miR-10b and miR-21 in U87 glioma cells. The up-regulated DEGs were found to be enriched in the cytokine-cytokine receptor interaction pathway (fig. S17A).

We isolated the DEGs in each of the enriched pathways, including PI3K-Akt, focal adhesion, and HIF-1 after knockdown of miR-21 and miR-10b (Fig. 4, C to E). Furthermore, to isolate the critical genes associated with GBM pathology and affected by simultaneous inhibition of miR-10b and miR-21, we intersected the down-regulated DEGs from PI3K-Akt, focal adhesion, and HIF-1 pathway (fig. S17B). We observed that vascular endothelial growth factor A (*VEGFA*) and protein kinase alpha C (*PRKCA*) were involved in all three selected pathways. Furthermore, 10 genes were common in the focal adhesion and PI3K-Akt pathways, while 3 genes were affected in both PI3K-Akt and HIF-1 pathways. Hence, we selected multiple genes including *VEGFA*, *PRKCA*, integrins (*ITGA10*, *ITGA11*, and *ITGB8*), platelet-derived growth factor receptors (*PDGFRA* and *PDGFRB*), angiopoietins (*ANGPT1* and *ANGPT2*), and interleukin-6 (*IL-6*), which have been reported to promote GBM progression, for additional validation. We also selected *IL-24* from the cytokine-cytokine interaction pathway for further evaluation. *IL-24* is the highest up-regulated DEG; it acts as a tumor suppressor with a potential role in overcoming TMZ resistance in GBM (*45*, *46*). The validation of the selected genes revealed notable down-regulation of *PDGFRB*, *VEGFA*, *ITGB8*, *ITGA10*, *ITGA11*, *PRKCA*, and *IL-6* in U87 cells in vitro after treatment with sγPNA BNPs (Fig. 4F). Western blot analysis also confirmed the down-regulation of VEGFA and PDGFR-β at the protein level in sγPNA BNP–treated U87 cells, whereas Scr-sγPNA BNP showed no impact (fig. S18). We also validated the selected genes in PDX (G22) cells and found a statistically significant down-regulation of *PDGFRB*, *ITGB8*, and *ITGA11* (Fig. 4G). *IL-24* was also found to be up-regulated in both U87 and G22 cells (fig. S19).

Off-target assessment of anti-seed γPNAs

The sγPNAs, because of their small length, could have perfect match binding regions in mRNAs, leading to off-target binding. Hence, we identified the mRNA sequences containing the seed region of miR-21 and miR-10b using blast analysis against the National Center for Biotechnology Information transcript reference sequences for humans (taxid: 9606). We selected the top 100 mRNA transcripts containing the miR-21 seed region (fig. S20, A
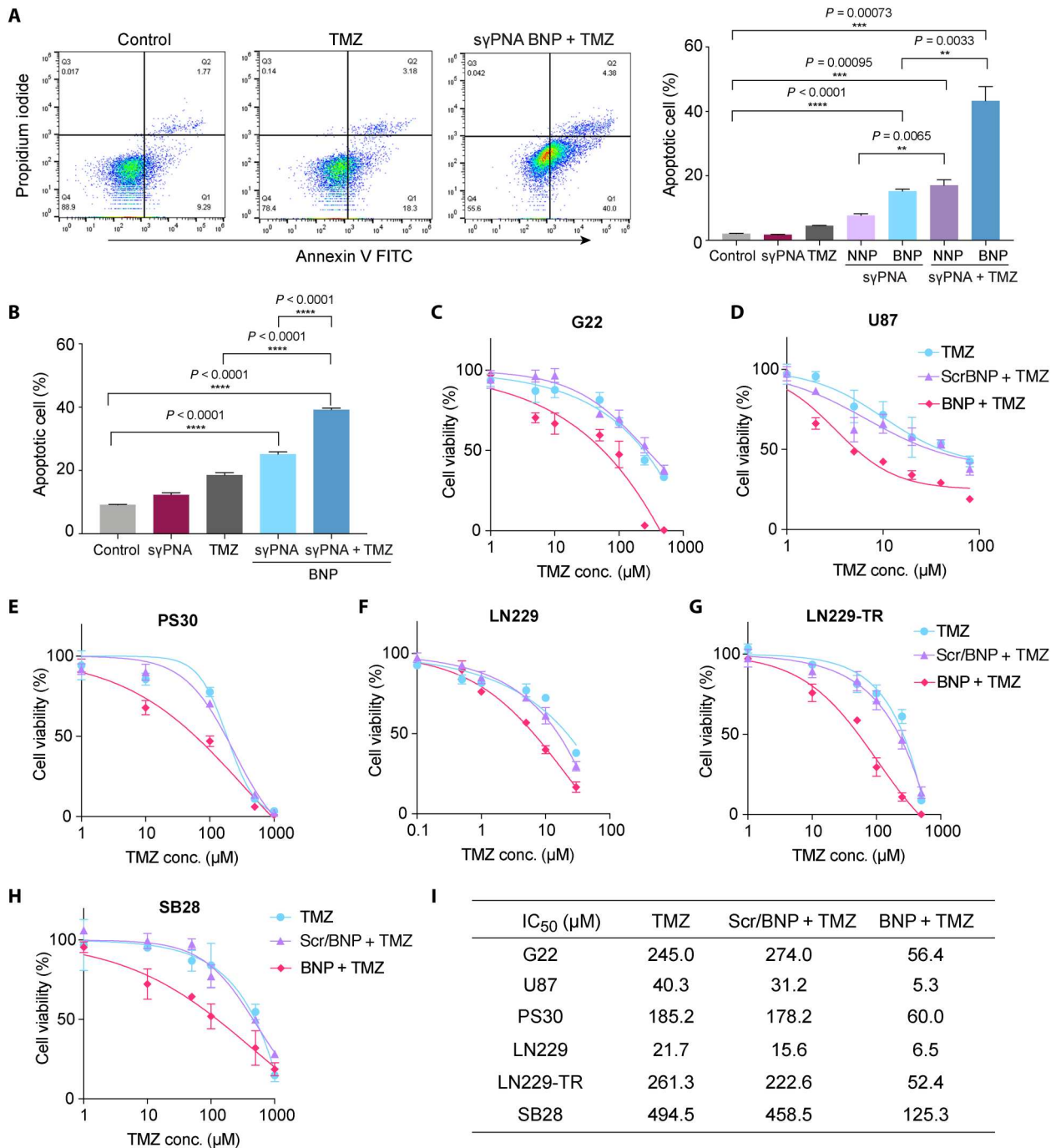
Fig. 3. Simultaneous knockdown of miR-21 and miR-10b sensitizes multiple glioma cells toward TMZ treatment. (**A**) Representative flow cytometry dot plots of apoptosis analysis in control, TMZ-treated, and sγPNA BNP + TMZ–treated U87 cells. Graph represents the percentage of early apoptotic cells after different treatments with sγPNA/NNP and BNP with or without TMZ. Data are expressed as means ± SD (n = 3). (**B**) Percentage of early apoptotic G22 cells after different treatments with sγPNA/BNP with or without TMZ. Data are expressed as means ± SD (n = 3). The cell viability of glioma cells, (**C**) G22 (PDX glioma cells), (**D**) U87 (human glioma cells), (**E**) PS30 (GBM-derived stem cells), (**F**) LN229 (human glioma cells), (**G**) LN229-TR (TMZ-resistant LN229 cells), and (**H**) SB28 (mouse glioma cells) after treatment with TMZ alone and in combination with BNP containing sγPNAs (sγPNA-21 and sγPNA-10b) or Scr/BNP containing scr-γPNAs (scr-γPNA-21 and scr-γPNA10b). Data are expressed as means ± SD (n = 3). (**I**) The IC$_{50}$ values of TMZ and combination treatment of TMZ with BNPs in multiple glioma cells. NNP indicates PLA-HPG NP, and BNP indicates PLA-HPG-CHO NP.
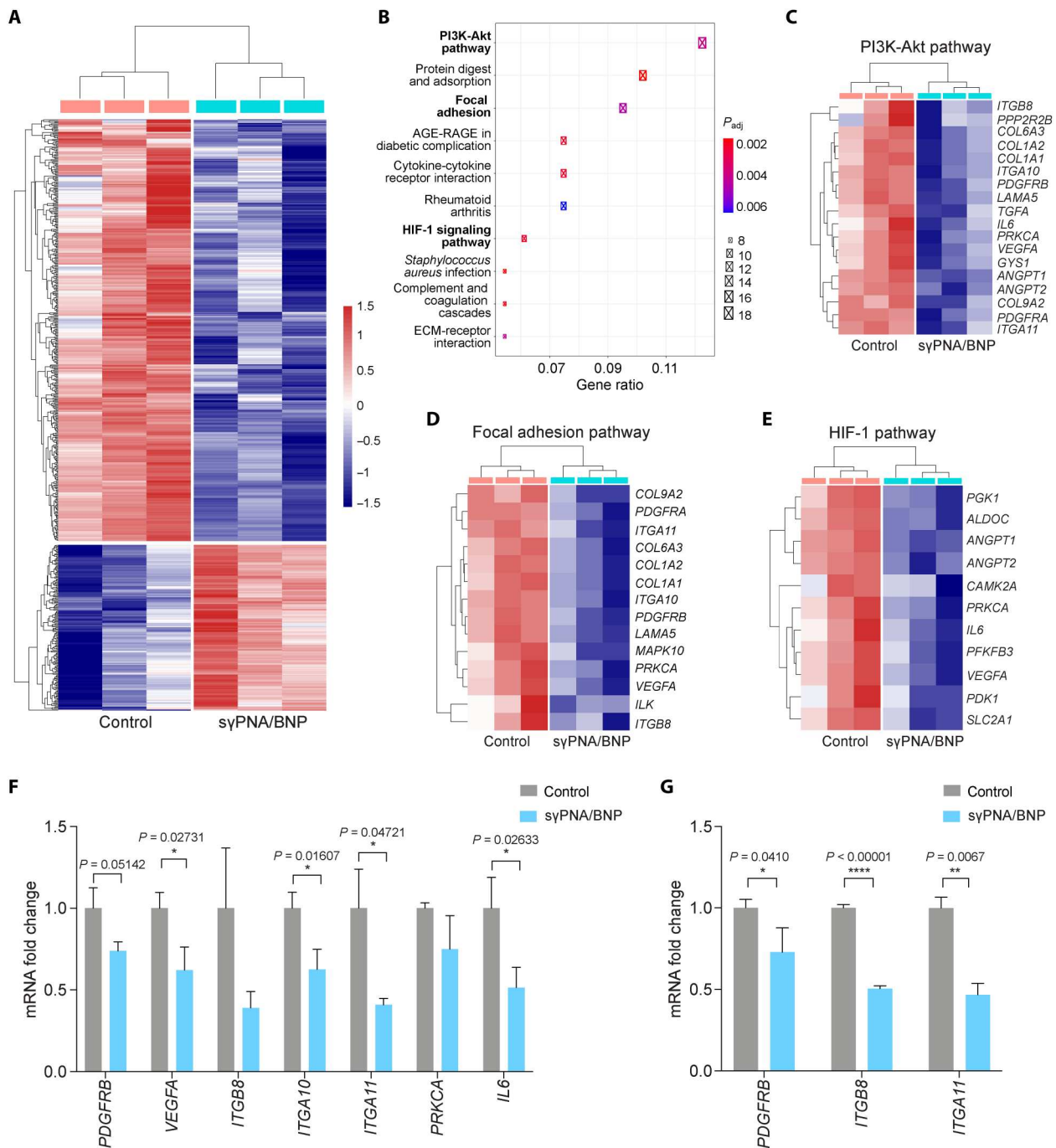
Fig. 4. γPNA/BNP–mediated knockdown of oncomiRs 21 and 10b affects PI3K-Akt, focal adhesion, and HIF-1 pathways to inhibit GBM progression. (**A**) Hierarchical clustering analysis of DEGs in U87 cells treated with sγPNA/BNP in comparison to control (untreated U87 cells). (**B**) Gene ontology analysis of differentially expressed down-regulated genes. (**C**) Heatmap of DEGs associated with the PI3K-Akt pathway. (**D**) Heatmap of DEGs associated with the focal adhesion pathway. (**E**) Heatmap of DEGs associated with the HIF-1 pathway. (**F**) Fold change in expression of the selected genes (*PDGFRB*, *VEGFA*, *ITGB8*, *ITGA10*, *ITGA11*, *PRKCA*, and *IL6*) from the PI3K-Akt, focal adhesion, and HIF-1 pathway via RT-PCR after treatment with sγPNA/BNP in U87 cells. (**G**) Fold change in the levels of *PDGFRB*, *ITGB8*, and *ITGA11* in G22 cells after treatment with sγPNA/BNP. Data are expressed as means ± SEM (*n* = 3). sγPNA/BNP indicates the physical mixture of sγPNA-21– and sγPNA-10b–loaded BNP. BNP indicates PLA-HPG-CHO NP.

and B), which led to the identification of 38 genes as potential off-target sites for sγPNA-21. Intersection of the isolated 38 genes with DEGs (606) obtained from the RNA-seq analysis showed <0.4% of DEGs with potential off-target activity for sγPNA-21 (fig. S20C). A similar analysis using the miR-10b seed region resulted in 39 genes (fig. S21, A and B), among which <0.5% were (fig. S21C) found in DEGs. These results suggest that we should expect minimal off-target activity of sγPNA-21 and sγPNA-10b.

Overexpression of miR-10b and miR-21 leads to poor survival of patients with GBM

To connect our findings with GBM in humans, we correlated the survival of GBM patients with the overexpression of miR-10b and miR-21. We found poor survival of patients with higher miR-21 levels but no impact of miR-10b levels on the survival of patients with GBM (fig. S22). However, when patients with higher expression of both miR-10b and miR-21 were examined, the survival probability was reduced to less than half when compared with low levels of miR-10b and miR-21 (fig. S23). These results indicate that up-regulation of both miR-10b and miR-21 contributes to aggressive growth and poor survival in GBM. Hence, the proposed strategy of targeting multiple oncomiRs can pave the way for personalized therapies for the treatment of GBM.

Tumor retention of sγPNA-loaded BNP after CED

To study the tumor retention and biodistribution of sγPNA loaded in BNP after CED, we infused TAMRA-labeled sγPNA/BNP into intracranial tumors and captured the fluorescence signal of TAMRA-sγPNA (Fig. 5A). As expected, a strong fluorescence signal was detected in the brain using in vivo imaging system (IVIS) 3 hours after CED (day 0.1), and brain cryosection images showed that sγPNA/BNP accumulated mainly in the tumor region after local delivery. After 1 day, we observed that sγPNA/

BNP distributed widely from the injection site and spread throughout the tumor region in the brain, as indicated by Ki67, a marker for cell proliferation (fig. S24A). After 7 days, comparatively less fluorescence was detected in the brain, but a visible signal was still retained in the tumor region until day 14, suggesting that sγPNA molecules were well retained in the tumor for up to 2 weeks after CED of sγPNA/BNP (Fig. 5B and fig. S24B). The CED of unencapsulated sγPNA at the same dose showed more than three-fold reduced signal than BNPs after 3 days, which decreased further with minimal fluorescence signal on days 7 and 14 (fig. S25). Thus, encapsulation of sγPNA into BNP provided sustained retention within the tumor region, which appears to be suitable for intracranial anti-miR treatment.

Improved survival in orthotopic GBM tumor model

The substantial tumor retention provided us a strong rationale to evaluate the therapeutic efficacy of the sγPNA/BNP in vivo. Intracranial U87 tumors were generated in immunocompromised mice, and NPs were administered via CED 6 days after tumor inoculation (Fig. 6A). The combination of sγPNA/BNP and TMZ was also evaluated by administering a single intraperitoneal injection of TMZ 1 day after CED infusion. In animals receiving sγPNA/BNP, median survival was increased to 53 days compared to the untreated control groups (45 days), confirming that miR inhibition mediated by sγPNAs effectively delayed tumor growth. Combination treatment of sγPNA/BNP and TMZ (25 mg/kg) greatly improved survival, and all the animals in this group ($n = 6$) survived until the study endpoint at 120 days. At the end of the study, animals receiving the combination treatment (TMZ and BNP) appeared to be tumor-free (day 120; movie S1), whereas control animals were found to be hunched because of tumor burden and neurological decline (day 46; movie S2). Administration of TMZ (25 mg/kg) prolonged the median survival to 81 days, confirming its therapeutic benefit,
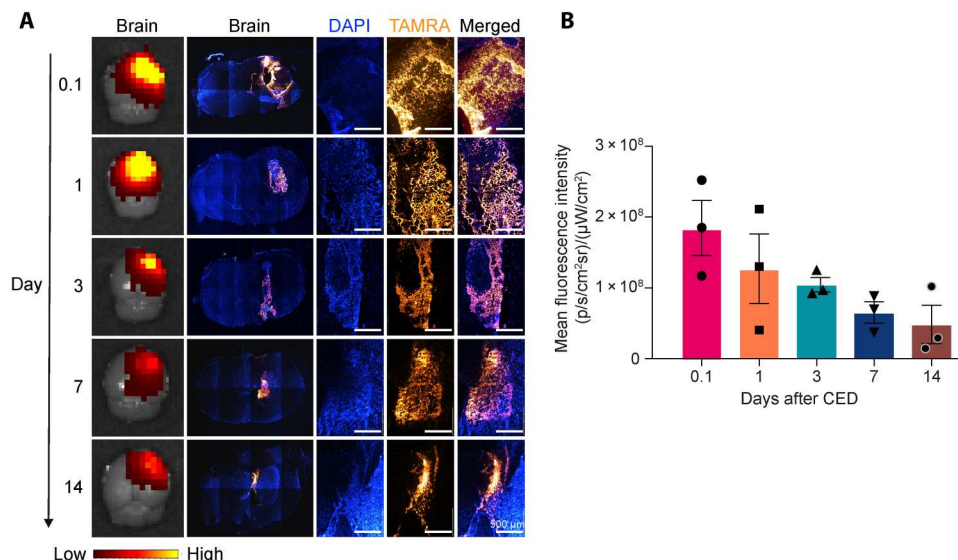

Fig. 5. Biodistribution of BNPs in U87 orthotopic mice model of GBM after CED. (**A**) From left to right, columns 1 and 2: IVIS and microscopic images of mice brain at days 0.1 (3 hours), 1, 3, 7, and 14 after CED of TAMRA-labeled sγPNA BNP into the tumor. CED was performed 10 days after tumor inoculation. Columns 3 to 5: Microscopic images showing the injection site of the brain sections at different time points with a higher magnification (10× objective). Nucleus is shown in blue (DAPI), and sγPNA (TAMRA) is shown in yellow. Scale bars, 500 μm. (**B**) Mean fluorescence intensity of TAMRA-sγPNAs in the brain IVIS images of (A) at different time points. Data are expressed as means ± SEM ($n = 3$ mice).
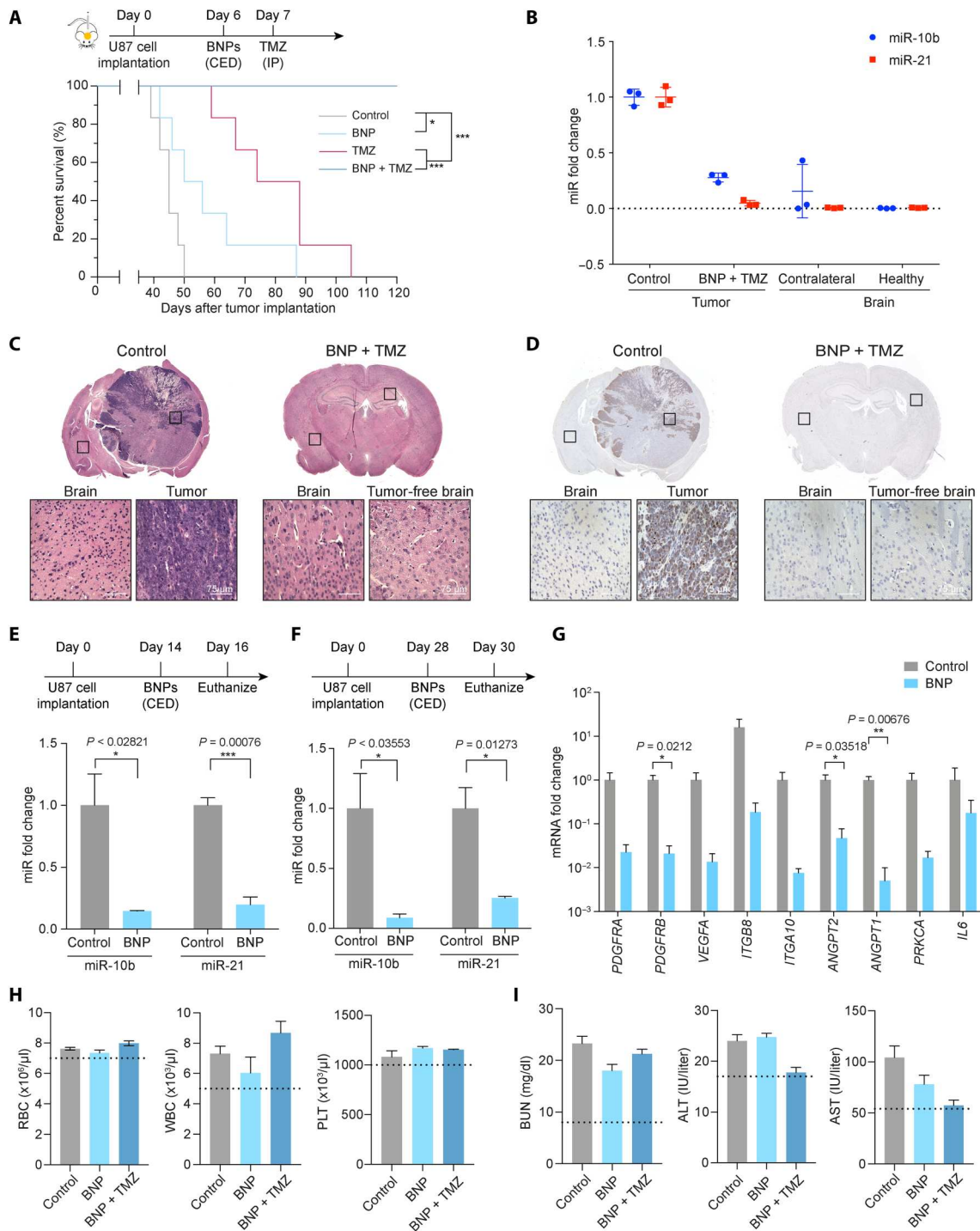
Fig. 6. The combination of sγPNA/BNP and TMZ improves the survival in an orthotopic mice model of GBM. (**A**) Survival of mice bearing U87-derived intracranial gliomas after treatment with sγPNA/BNP, TMZ, and the combination of sγPNA/BNP with TMZ. NPs were administered by CED at a dose of 200 mg/ml, and TMZ was administered intraperitoneally at a dose of 25 mg/kg. (**B**) The levels of miR-21 and miR-10b in gliomas of control and sγPNA/BNP + TMZ–treated mice at the end of the survival study. Results are represented as means ± SD ($n = 3$ mice). The control tumor tissues were harvested after animal euthanasia, and treated mice brain tissues were harvested on day 120. (**C**) H&E staining of control (day 46) and sγPNA/BNP + TMZ–treated mice brain (day 120) at the end of the survival study. Scale bars, 75 μm. (**D**) Ki67 staining of control (day 46) and sγPNA/BNP + TMZ–treated mice brain (day 120) at the end of the survival study. Scale bars, 75 μm. The levels of miR-10b and miR-21 in mice gliomas 48 hours after CED of sγPNA/BNP on (**E**) day 14 and (**F**) day 28. Results are represented as means ± SD ($n = 3$ mice). (**G**) The gene expression levels of *PDGFRA*, *PDGFRB*, *VEGFA*, *ITGB8*, *ITGA10*, *ANGPT2*, *ANGPT1*, *PRKCA*, and *IL6* in tumors 48 hours after CED on day 28. (**H**) Clinical chemistry of blood samples including white blood count (WBC), platelets (PLT), and red blood cells (RBCs) from mice after 48 hours of sγPNA/BNP and sγPNA/BNP + TMZ administration. (**I**) Blood biochemistry including BUN, ALT, and AST from mice after 48 hours of sγPNA/BNP and sγPNA/BNP + TMZ treatment. (G to I) Results are represented as means ± SEM ($n = 3$ mice). sγPNA/BNPs are a physical mixture of sγPNA-21 BNP and sγPNA-10b BNP. BNP indicates PLA-HPG-CHO NP.

but TMZ alone was less effective than the combination with sγPNA/BNP. Furthermore, animals treated with lower doses of TMZ (12.5 mg/kg) did not provide any improvement ($P = 0.0853$) in survival compared to the control group (fig. S26), whereas the same dose of TMZ combined with sγPNA/BNP extended survival time over 100 days. These results indicate that sγPNA/BNP in combination with TMZ produced the longest survival time by successfully suppressing tumor growth and sensitizing the tumor cells to TMZ. Analysis of hematoxylin and eosin (H&E) and Ki67 brain sections of one survivor that received combination treatment (brain collected on day 120) and one untreated control animal (brain collected on day 46) showed the presence of a fully developed tumor localized within the brain of the untreated mouse [Fig. 6, C and D (left)]. The tumor is characterized by a densely cellular mass lesion composed of highly atypical, pleomorphic neoplastic glial cells that display high proliferative activity. The animal in the sγPNA/BNP combination treatment group instead shows normal cerebral cytoarchitecture devoid of neoplastic cells and no evidence of tumor [Fig. 6, C and D (right)]. Furthermore, proliferative activity is only seen in neoplastic cells, whereas the combination-treated brain shows no cell division, which is typical for a normal adult brain.

In vivo knockdown of miR-10b and miR-21
At the end of the tumor survival study (day 120), we measured the relative levels of miR-10b and miR-21 in the brain tissues around the injection site of sγPNA/BNP and TMZ treatment group (Fig. 6B). Untreated mice tumors were collected after animal euthanasia and measured as a comparison. Compared to the control group, animals in the combined treatment group showed 72% knockdown of miR-10b and 95% decrease in miR-21 expression in the brain tissues ipsilateral to the injection site, indicating successful oncomiR inhibition mediated by sγPNA/BNP and TMZ. The expression levels of miR-10b and miR-21 in the contralateral hemisphere and healthy mice brains were also measured as comparisons.

To further investigate the role of sγPNA/BNP in oncomiR inhibition, we performed two separate experiments where sγPNA/BNP was administered 14 or 28 days after tumor implantation after the treatment schedule indicated in Fig. 6 (E and F, respectively). Tissues at the tumor site were harvested to examine the expression levels of oncomiRs. Quantitative polymerase chain reaction (PCR) results revealed that sγPNA/BNP treatment resulted in statistically significant down-regulation of miR-10b and miR-21 in tumors at different growth stages, further confirming efficient suppression of both targets (Fig. 6, E and F). In addition, among the genes selected from RNA-seq analysis, *PDGFRA*, *PDGFRB*, *VEGFA*, *ITGB8*, *ITGA10*, *ANGPT1*, *ANGPT2*, *PRKCA*, and *IL-6* showed reduced levels in treated tumors after 14 days (fig. S27) and 28 days (Fig. 6G) of tumor implantation.

Toxicity assessment of sγPNA/BNP and TMZ
We assessed the toxicity of different treatments by performing complete blood count, blood biochemistry, and histopathological analysis. As shown in Fig. 6H and fig. S28, sγPNA/BNP alone and in combination with TMZ did not alter white blood cell, platelet, red blood cell, or other blood components when compared with control animals after 48 hours of treatment. No difference was found in liver enzymes [alanine aminotransferase (ALT), aspartate transaminase (AST), lactate dehydrogenase (LDH), and alkaline phosphatase] and renal function markers [blood urea nitrogen (BUN) and creatinine] in mice after receiving treatments (Fig. 6I and fig. S29). An independently conducted pathological analysis found no obvious tissue changes in the treated animals from the survival study when compared to control animals upon examination of the H&E-stained major organs (fig. S30). Overall, these data confirm the safety of sγPNA/BNP in combination with TMZ.

Improved survival in PDX mice model
We tested the efficacy and safety of this combination strategy on patient-derived GBM (G22) cells. The PDX orthotopic tumor model was established by injecting G22 cells intracranially in immunocompromised mice, as previously described (47), and treatments were performed as described above. sγPNA/BNP combined with TMZ (25 mg/kg) greatly prolonged survival, and 80% of animals survived to the study endpoint at 120 days (one died on day 90; $n = 5$) (Fig. 7A). Animals receiving combination treatment that survived until the end of the study exhibited normal physical activity in comparison to untreated control animals, which had signs of morbidity as early as day 39 due to tumor development (movies S3 and S4). Histological analysis of H&E- and Ki67-stained sections confirmed that the brains of surviving BNP plus TMZ–treated animals were tumor-free 120 days after tumor inoculation (Fig. 7, C and D). Animals receiving sγPNA/BNP treatment or a single dose of TMZ (25 mg/kg) only extended median survival to 69 and 79 days, respectively, compared to the untreated controls (51 days), much less than the combination of sγPNA/BNP with TMZ. In vivo knockdown efficiency was also assessed on the PDX model. The relative levels of miR-10b and miR-21 at the end of the survival study (day 120) were found to be low and comparable to those in the contralateral hemisphere and healthy mice brains (Fig. 7B). Efficient knockdown of miR-10b (99%) and miR-21 (92%) was observed in the animals treated by sγPNA/BNP combined with TMZ. Substantial down-regulation of miR-10b and miR-21 in the tissue at the tumor site was observed when the administration of sγPNA/BNP was performed 14 or 28 days after tumor implantation (Fig. 7, E and F). Similarly, the expression of 10 down-regulated genes identified from RNA-seq analysis—*PDGFRA*, *PDGFRB*, *VEGFA*, *ITGB8*, *ITGA10*, *ITGA11*, *ANGPT1*, *ANGPT2*, *PRKCA*, and *IL-6*—was notably lower in treated animals than in the untreated controls (Fig. 7G). Collectively, we found that sγPNA-loaded BNP resulted in successful inhibition of miR-10b and miR-21 and substantial improvement in animal survival in orthotopic PDX animals, consistent with our findings on intracranial U87 tumors.

Complete blood counts, blood biochemistry, and histopathological analyses were conducted to evaluate toxicity. Figures S31 and S32 showed no difference between the treated animals and controls in terms of blood components and liver enzymes (ALT, AST, and LDH) and renal function markers (BUN and creatinine). H&E-stained sections of multiple organs, including liver, spleen, kidney, cardiac muscle, and lung, also showed no differences between treated animals and untreated controls from the survival study in terms of inflammation or cell death (fig. S33).

DISCUSSION
Despite considerable attention in preclinical and clinical research, GBM remains an aggressive disease, with limited survival and poor treatment options (48, 49). Little progress has been made
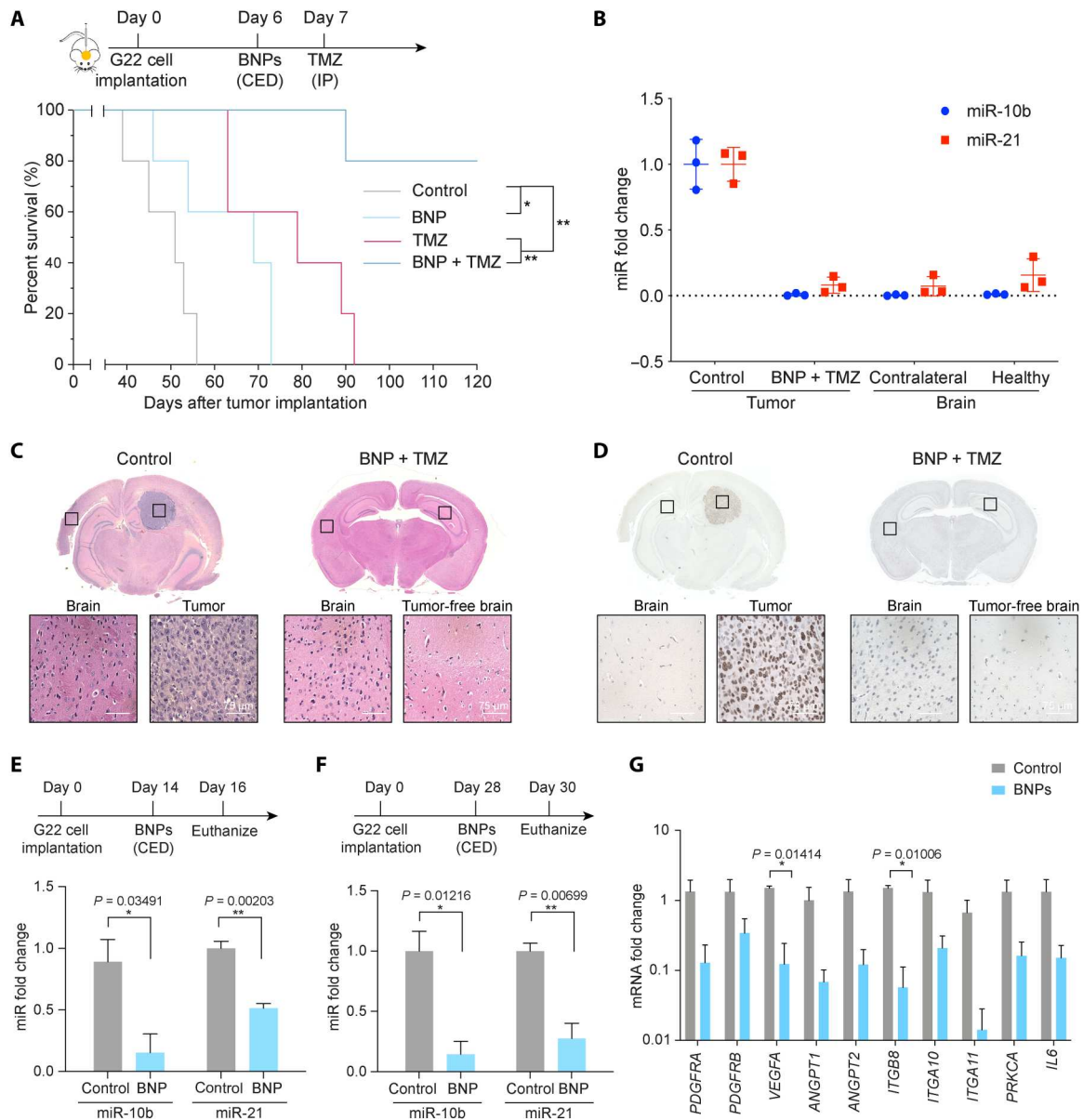
Fig. 7. Efficacy of targeting oncomiRs 10b and 21 via BNP-delivered sγPNAs in a PDX mice model of GBM. (**A**) Survival of mice-bearing patient (G22)–derived intracranial gliomas after treatment with BNPs containing sγPNA, TMZ, and the combination treatment of BNP with TMZ. BNPs were administered by CED at a dose of 200 mg/ml, and TMZ was administered intraperitoneally at a dose of 25 mg/kg. (**B**) The levels of miR-21 and miR-10b in gliomas of control and BNP + TMZ–treated mice at the end of the survival study. Results are represented as means ± SD ($n = 3$ biologically independent animals). The control tumor tissues were harvested after animal euthanasia, and treated mice brain tissues were harvested on day 120. (**C**) Histology of H&E-stained control and BNP + TMZ–treated mice brain at the end of the survival study. Control mouse brain was harvested on day 39, and sγPNA/BNP + TMZ–treated mouse brain was harvested on day 120. Scale bars, 75 μm. (**D**) Ki67 staining of control and BNP + TMZ–treated brain at the end of the survival study. Control mouse brain was harvested on day 39, and sγPNA/BNP + TMZ–treated mouse brain was harvested on day 120. Scale bars, 75 μm. (**E**) The expression levels of miR-10b and miR-21 in mice gliomas 48 hours after CED of NPs on day 14 and (**F**) day 28 after tumor implantation. Results are represented as means ± SEM ($n = 3$ biologically independent animals). (**G**) The levels of downstream genes *PDGFRA*, *PDGFRB*, *VEGFA*, *ITGB8*, *ITGA10*, *ITGA11*, *ANGPT2*, *ANGPT1*, *PRKCA*, and *IL6* in mice gliomas 48 hours after CED of NPs on day 28. Results are represented as means ± SEM ($n = 3$ biologically independent animals). sγPNA/BNPs are a physical mixture of sγPNA-21 BNP and sγPNA-10b BNP. NNP indicates PLA-HPG NP, and BNP indicates PLA-HPG-CHO NP.

toward improved survival outcomes in patients with GBM over the standard of care, which includes surgical resection and radiation therapy plus TMZ (50, 51). Reasons for this failure include the lack of powerful therapeutic agents, restricted entry of drugs into intracranial tumors because of the blood-brain barrier (BBB), and tumor heterogeneity driven by multiple coordinated signaling pathways. All of these issues present challenges for GBM therapy (52). Here, we sought to investigate a potential solution that would involve an addition to the standard of care: infusion of highly effective sγPNA anti-miRs directly into tissue harboring tumor cells, with the sγPNAs packaged into NPs that are taken up in tumor cells. This strategy was targeted at two GBM-specific oncomiRs to overcome intrinsic resistance to the induction of cell death.

Several chemically modified oligonucleotides (anti-miRs) exhibiting enzymatic stability and high binding affinity have been explored in the past for targeting oncomiRs, including locked nucleic acid (53), 2-O-methyl oligonucleotides (54), morpholinos (55), and PNAs (26). On the basis of their metabolic stability and binding affinity, PNA oligomers are efficient agents to inhibit the function of miRs. Modification of PNAs at the γ position can address many of the shortcomings of conventional PNAs, further maximizing the antagonizing effect on the function of target miR (28). Here, we designed short serine-γPNAs conjugated with cationic arginine residues. Gel shift assays showed that the synthesized sγPNAs (sγPNA-21 and sγPNA-10b) bind with the respective miR, indicating specific and strong affinity for target oncomiRs. The sγPNAs encapsulated in BNPs exhibited a greater miR inhibition effect in comparison with nonmodified full-length PNAs loaded in the same carrier. These short γPNA oligomers have enhanced hybridization due to their γ modification and cationic residues, and we predicted that they would improve the therapeutic efficacy.

In addition to efficacy, delivery of next-generation anti-miRs to the central nervous system remains an enormous challenge that needs to be resolved. The efficacy of GBM therapies is limited by the presence of BBB (56); however, local delivery approaches have been beneficial to achieve intracranial distribution. Unlike diffusion-based methods (57), CED uses positive pressure flow and a catheter to achieve stereotactic placement and direct infusion of drugs into the tumor resection cavity, providing large distribution volumes (58). In addition to intracranial delivery, high interstitial distribution can be achieved by adjusting the flow, distribution can be monitored in real time, and antitumor efficacy can be achieved at low doses, hence minimizing neurotoxicity and systemic toxicity (59). CED has been used in multiple clinical trials for intracranial delivery of chemotherapeutics (60), antisense oligonucleotides (61), and liposomal vectors for gene therapy (62). In addition, CED has been investigated at nonclinical and preclinical stages for the delivery of NPs (63) and viral vectors (64) for the treatment of gliomas. Notably, recent clinical trials suggest that CED is safe and feasible, but present therapeutic approaches fail to improve the survival of patients with GBM (34). Several technical factors such as catheter design and placement, backflow, target heterogeneity, edema, flow rate, volume of distribution, and infusion volume have emerged as the major limitations for the clinical success of CED (65, 66). The failure of the phase 3 PRECISE clinical trial using CED for recurrent GBM was attributed to improper catheter positioning, which resulted in poor drug distribution (67). However, these challenges have also led to improvements in technology and implementation (68), which have allowed for recent

successes (69, 70). We believe that our approach, which allows for the sustained activity of unique compounds that synergize with current therapy, adds to the likelihood of success in the future. Most drugs have short brain half-lives and are eliminated quickly after the infusion stops. We believe that infusion of NPs can improve the current CED strategies (71), as NPs offer improved brain retention and sustained drug release for days to weeks after the end of infusion.

To achieve efficient cellular delivery, the sγPNAs were encapsulated in PLA-HPG NPs. We previously demonstrated that NPs composed of PLA-HPG (NNP) and a bioadhesive version, PLA-HPG-CHO (BNP), are safe and advantageous for the delivery of PNAs to the brain (18, 38). Here, we also observed a four- and two-fold increase in cellular uptake with sγPNA-loaded BNPs in two GBM cell lines, U87 and G22, respectively, over free sγPNAs. The preferential association of BNP with tumor cells also resulted in an enhanced oncomiR suppression in vitro analyzed by quantitative real-time PCR (qRT-PCR). The expression of both miR-10b and miR-21 was substantially down-regulated after sγPNA NP treatment. We hypothesize that altered miR levels in tumor cells might affect the expression of gene products that stimulate cell proliferation or that induce apoptosis, blocking tumor cells from developing into a proliferative state.

High-throughput profiling revealed the overexpression of miR-10b and miR-21 in a large portion of human gliomas (22). On the basis of the specific molecular aberrations in GBM tumors, we designed sγPNAs targeting these two oncomiRs and prepared formulations loaded with sγPNA oligomers. Upon simultaneous inhibition of both targeted miRs in vitro, we observed effective cell apoptosis in glioma cells treated by sγPNA/NP. More than 40% of apoptotic-associated cell death was achieved by exposure to sγPNA/BNP (2 mg/ml) on two different GBM cells. These results suggested modest anticancer activity mediated by miR inhibition in tumor cells. RNA-seq analysis revealed that coinhibition of miR-21 and miR-10b induces substantial down-regulation of genes from PI3K-Akt, HIF-1, and focal adhesion pathways. We hypothesize that alterations in these proliferative pathways sensitize glioma cells toward TMZ-mediated cell death. We noticed that TMZ combined with sγPNA NPs induced a larger degree of cell apoptosis than TMZ or NPs alone. Therefore, we evaluated the cell killing activity of this combination strategy via cell survival assays in vitro, speculating improved chemosensitivity in treated tumor cells. As expected, combination with sγPNA/BNP effectively promoted tumor cell responses to TMZ, with reduced cell viability than with TMZ alone on six GBM cell lines, including human GBM cells (U87 and LN229), PDX cells (G22), glioma stem cells (PS30), TMZ-resistant cells (LN229-TR), and mouse glioma cells (SB28). Furthermore, this sensitization effect to chemotherapy mediated by sγPNA/BNP acted in a synergistic manner, as analyzed by the additive model on U87 cells (observed/expected ratio = 0.644; table S2) (72, 73). Tumor cell–specific cytotoxicity was also observed in this combination treatment, which displayed limited toxicity against healthy cells.

Limited therapeutic options, the presence of BBB, and the lack of progress in systemic delivery motivated more direct approaches for GBM therapy, such as local delivery via CED (74, 75). Wide distribution of truly effective agents by CED is expected to influence the overall therapeutic outcomes. With this in mind, CED of sγPNA encapsulated in BNP was used to improve intracranial drug

distribution and prolong the survival of tumor-bearing animals. We observed up to 2-week retention and widespread distribution of sγPNA/BNP within the intracranial tumor after CED infusion. This is consistent with our recently reported results where BNPs led to the persistent presence of encapsulated camptothecin (~50%) in the squamous cell carcinoma tumor at 10 days after intratumoral injection (*41*). We attribute the markedly improved tumor retention to the enhanced association with tumor cells provided by the bioadhesive surface of the aldehyde-rich BNP. On the basis of our in vitro and in vivo results, we believe that BNP-mediated increased tumor cell internalization and sustained drug release bring advantages to localized drug delivery and GBM therapy, particularly for invasive clinical approaches. Moreover, longer tumor retention is critically important when nucleic acid therapies are combined with other approaches (such as chemotherapy and radiotherapy), which require multiple doses over time.

In our survival study, CED of sγPNA-loaded BNP plus a single dose of TMZ prolonged the survival time of animals bearing intracranial U87 tumors and patient-derived G22 tumors. Although each of the monotherapies, sγPNA/BNP, and TMZ alone showed some effect in delaying tumor progression and extending median survival, neither of them was able to completely inhibit tumor growth. Here, we showed that all the U87 tumor–bearing animals receiving sγPNA/BNP plus TMZ treatment were tumor-free long survivors (>120 days); this robust antitumor activity could be beneficial for lowering the systemic drug dose. For example, sγPNA/BNP combined with a reduced dose of TMZ (12.5 mg/kg) successfully increased the survival time of tumor-bearing animals to more than 100 days. Similar therapeutic benefits were reproduced on patient-derived GBM tumors, thus leading to improved animal survival ($P < 0.0018$, versus control). We hypothesize that suppression of key oncotargets (miR-10b and miR-21) by anti-miR sγPNAs enhances the sensitivity of tumor cells to chemotherapy, resulting in an elevated response to TMZ treatment. Future studies should focus on evaluating the efficacy of BNPs in syngeneic mice models of GBM, which better recapitulates the tumor microenvironment and immunogenicity (*76*). It will also allow for testing the efficacy of BNPs in combination with emerging immunotherapies. Although we did not notice any toxic response in both U87 and G22 mice models of GBM, it is critical to evaluate the safety of BNPs and TMZ in immunocompetent mice models to ensure successful clinical translation of the proposed strategy.

In conclusion, we propose a therapeutic approach to deliver anti-miR sγPNA-loaded BNP with bioadhesive surface modifications via CED to intracranial GBM tumors. Two oncomiRs, miR-10b and miR-21, were targeted simultaneously, resulting in cooperative oncomiR inhibition and sensitization of tumors to TMZ treatment. Combined anti-miR sγPNA NPs with TMZ resulted in a remarkable delay of tumor growth and prevention of disease relapse. Thus, our translational strategy, which builds on the current standard of care, may improve GBM therapeutic outcomes.

MATERIALS AND METHODS
Material
PLA (M_w = 20.2 kDa and M_n = 12.4 kDa) was purchased from Lactel. Ethyl acetate, acetonitrile, and dimethyl sulfoxide (DMSO) were obtained from J.T. Baker. TMZ was obtained from Enzo Life Sciences. Human GBM cell lines U87 was obtained from the American Type Culture Collection, and human astrocyte and human GBM cell lines LN229 and TMZ-resistant LN229-TR were provided by T. Lee at Yale. G22 (PDX) cells were obtained from J. Sarkaria (Mayo Clinic, Rochester, MN). PS30 (GBM-derived) stem cells were obtained from J. Zhou at Yale. Mouse glioma SB28 cells were provided by J. Vasquez at Yale and obtained from H. Okada (University of California, San Francisco). The cells were grown in Dulbecco's modified Eagle's medium (Invitrogen) supplemented with 10% fetal bovine serum and 1% penicillin-streptomycin and cultured at 37°C with 5% CO_2 in a humidified chamber.

Methods
Synthesis of PNA oligomers
PNAs were synthesized via solid-phase synthesis using 4-methylbenzhydrylamine resin and standard Boc chemistry procedures as reported previously (*77*). Regular Boc monomers and serine-γPNA-Boc monomers (A, T, C, and G) purchased from ASM Chemicals and Research (Germany) were used. Three arginine residues were conjugated to the N terminus or 5′ end of PNAs. TAMRA dye, bought from VWR (Pennsylvania, USA), was further conjugated to the 5′ end with a Boc-MiniPEG-3 linker in between. After completion of synthesis, PNAs were cleaved from the resin using trifluoroacetic acid:trifluoromethanesulfonic acid:m-cresol: thioanisole at a ratio of 6:2:1:1 as cleavage cocktail and precipitated using diethyl ether. PNAs were further purified using RP-HPLC to obtain the pure fractions. The molecular weight of purified PNAs was confirmed using matrix-assisted laser desorption/ionization–time-of-flight spectrometry. The concentration of PNAs in water was determined using ultraviolet-visible spectroscopy. The amount of PNA was then calculated using the extinction coefficient of PNA obtained by combining the extinction coefficient of individual monomers of the sequence.

Gel shift assay
The binding of PNAs with the target oncomiRs 10b and 21 was determined by incubating PNAs with the target in a buffer simulating physiological ionic conditions (10 mM NaPi, 150 mM KCl, and 2 mM $MgCl_2$) at 37°C for 16 hours in a thermal cycler (Bio-Rad, USA). The samples were separated using 10% nondenaturing polyacrylamide gel and tris/boric acid/EDTA buffer at 120 V for 35 min. For detection of bound and unbound fractions of target oncomiRs, gels were stained using SYBR-Gold (Invitrogen, USA) followed by imaging in a Gel Doc EZ imager (Bio-Rad, USA).

NP preparation
sγPNA/NNP. sγPNA-loaded NNPs were prepared using the emulsion-evaporation method as previously reported. Fifty milligrams of polymer (PLA-HPG) was dissolved in 2.4 ml of ethyl acetate overnight. sγPNA (50 nmol) was dissolved in 0.6 ml of DMSO and then added to the polymer solution, obtaining a PNA/polymer mixture. The resulting solution was added dropwise to 2 ml of deionized (DI) water under a strong vortex and then sonicated for 10 s for four cycles. The emulsion was diluted in 20 ml of DI water and concentrated in a rotovap for 20 min. The particle solution was transferred to an Amicon centrifugal filter unit (100 kDa) and washed twice by water. Last, the obtained particles were resuspended in DI water and snap-frozen in aliquots. sγPNA-21–loaded NNP and sγPNA-10b–loaded NNP were mixed at a 1:1 molar ratio to obtain sγPNA/NNP before further use. Scr-sγPNA and regular PNA-loaded NNPs were prepared using the same method.

sγPNA/BNP. To create sγPNA/BNP, sγPNA/NNP (25 mg/ml; as above) was incubated with 0.1 M NaIO$_4$ (aq) and 10× PBS (1:1:1, v:v) for 20 min on ice. NaSO$_3$ (0.2 M) at 1:1 (v/v) ratio was added to quench the reaction. The particle solution was washed with water at 13,000 relative centrifugal field (rcf) using a centrifugal filter unit (Amicon, 100 kDa) and resuspended in DI water. Regular PNA-loaded BNPs were synthesized with the same method.

NP characterization

Transmission electron microscopy. For TEM imaging, 2 μl of particles (20 mg/ml) was applied on a CF400-CU grid (Electron Microscopy Sciences) for 1 min. Extra liquid was carefully removed, and the grid was stained by one drop of NANO-W (Nanoprobes) for 1 min. Liquid was removed, and the sample was air-dried before imaging. Images were obtained using Tecnai Osiris (FEI).

Size and ζ potential. The hydrodynamic diameter of NPs was measured by DLS using a Malvern Nano-ZS (Malvern Instruments). NPs were diluted to 0.2 mg/ml with DI water before measurement. The same particle solution was loaded into a disposable capillary cell to measure the ζ potential on the Malvern Nano-ZS.

Size stability in aCSF. Particle solutions were incubated in aCSF (Harvard Apparatus) at 37°C and measured by DLS at designated time points.

sγPNA loading and release. Particle suspension (100 μl) was lyophilized in a preweighed tube to measure NP yield. Following lyophilization, NPs were dissolved in acetonitrile and incubated for 24 hours at room temperature. Absorbance at 260 nm was read by a NanoDrop 8000 (Thermo Fisher Scientific) to measure sγPNA loaded in the NPs. Scr-sγPNA and regular PNA loading efficiencies were determined using the same method. Release profile of sγPNA from different NP formulations was analyzed by incubating 10 mg of NPs in 1 ml of PBS (pH 7.4) in a shaking incubator at 37°C. At predetermined time points, aliquots were taken out and centrifuged using an Amicon centrifugal filter unit (100 kDa). Filtrates were collected for analysis.

Cellular uptake of sγPNA-loaded NPs

Cells were seeded in 24-well plates at a density of 50,000 cells per well and incubated with either 0.5 mg/ml of NP or the same concentration of free sγPNA for 24 hours. sγPNA oligomers used in this experiment were labeled with TAMRA for fluorescent evaluation. The cells were harvested, and cell uptake was determined from TAMRA fluorescence per cell using an Attune NxT (Invitrogen) flow cytometer and FlowJo software for data analysis. For microscopic observation, U87 cells were cultured in a 20-mm glass-bottom dish (20,000 cells per dish) before treatments. Cells were exposed to NPs (1 mg/ml) or free sγPNA for 24 hours and washed with PBS after treatments. After 4% paraformaldehyde fixation, cells were stained with Alexa Fluor 488 phalloidin (Life Technologies) and 4′,6-diamidino-2-phenylindole (DAPI) and observed by a SP5 confocal microscope (Leica).

Quantitative real-time polymerase chain reaction

The knockdown of miR-10b and miR-21 was analyzed by qRT-PCR. Cells were seeded in 24-well plates at a density of 200,000 cells per well. Cells were treated with various formulations at a PNA concentration of 300 nM. Scr-sγPNA–loaded NPs and regular PNA-loaded NPs with the same total PNA concentration were applied as control groups. After 72 hours, total RNA was extracted using the mirVana miRNA Isolation Kit (Ambion). The Advanced miRNA cDNA Synthesis Kit (Thermo Fisher Scientific) was used for cDNA synthesis. TaqMan PCR reactions were performed

with TaqMan fast advanced master mix (Thermo Fisher Scientific) and TaqMan Advanced miRNA assays (Thermo Fisher Scientific) for miR-10b, miR-21, and miR-26b analysis. miR levels were quantified using a CFX Connect Real-Time PCR Detection System and CFX Manager Software (Bio-Rad). Relative expression was calculated according to the comparative threshold cycle (Ct) method and normalized by miR-26b. For the evaluation of *PTEN* mRNA level, PCR reactions were performed using *PTEN* and *GAPDH* TaqMan Gene Expression Assays (Thermo Fisher Scientific) and quantified with the CFX Real-Time PCR Detection System and CFX Manager Software. The results were calculated with Ct method and normalized by *GAPDH*.

Annexin V assay

Apoptosis was assessed using the FITC Annexin V Apoptosis Detection Kit (BD Pharmingen). The excitation/emission peak of FITC (fluorescein isothiocyanate) is 491/516 nm and that of PI is 535/615 nm, which does not overlap with TAMRA′s emission wavelength peak (552/578 nm). Briefly, tumor cells were plated in 24-well plates at a density of 200,000 cells per well. The cells were treated with free sγPNA, sγPNA-loaded NPs, and/or TMZ for 72 hours (200 nM sγPNA-21, 200 nM sγPNA-10b, and 40 μM TMZ). The FITC annexin V apoptosis detection was performed using flow cytometry in accordance with the manufacturer′s protocol, and the data were processed using FlowJo. FITC annexin V–positive and PI-negative cell populations were identified as early apoptotic cells. Cells that stain positive for both FITC annexin V and PI are either in the end stage of apoptosis or are undergoing necrosis. Cells that stain negative for both dyes are identified as alive.

Caspase 3/7 activity evaluation

U87 cells were plated in 96-well plates at a density of 5000 cells per well and treated with various sγPNA NP formulations and TMZ (200 nM sγPNA-21, 200 nM sγPNA-10b, and 40 μM TMZ). Treatments were removed 48 or 72 hours later, and enzymatic activities of caspase 3 and 7 were measured using Caspase-Glo 3/7 Assay (Promega) and read by a microplate reader (SpectraMax M5).

Cell viability assay

Cells were seeded in 96-well plates at a density of 5000 cells per well and treated with increasing concentrations of NP formulations. Cell viability was evaluated by CellTiter-Glo Luminescent Cell Viability Assay (Promega) after 48 and 72 hours of treatment. Luminescence was measured using a plate reader (SpectraMax M5), and relative cell viability was normalized to the viability of untreated cells. For TMZ-involved combination studies, cells were seeded in 96-well plates at a density of 1000 cells per well (U87, G22, LN229, and LN229-TR) and exposed to Scr-sγPNA/BNP and sγPNA/BNP. PS30 cells, nonadherent cells with slower growth rate, were seeded at a density of 3000 cells per well followed by NP treatment. After 48 hours, NPs were removed, and TMZ was added to the wells. Cell viability was measured as described above after 5 days of treatment. The data were analyzed and plotted with Prism 9.

RNA sequencing

U87 cells were seeded in 24-well plates at a density of 50,000 cells per well and cultured overnight before use. sγPNA-21/BNP (150 nM sγPNA-21), sγPNA-10b/BNP (150 nM sγPNA-10b), and sγPNA/BNP (150 nM sγPNA-21 and 150 nM sγPNA-10b) were added to cells and incubated for 72 hours. Total RNA from each sample was extracted using the mirVana miRNA isolation kit. The libraries were made using Illumina TruSeq Stranded mRNA

library preparation. The sequencing was done with 45 to 50 M total 75–base pair paired-end reads using Illumina NextSeq 500.

Analysis of RNA-seq data

Total counts per gene were quantified and used in further analysis. All downstream analyses were accomplished by R (3.6.3). DEGs between different groups were identified by the package DESeq2 (1.26.0) with a filtering criteria of fold change ≥ 1.5 and P_{adj} < 0.05 (78). The package cluster profiler (3.14.3) was used to identify specific pathways overrepresented in the DEGs, and significant pathways were picked out by setting P value cutoff = 0.05 and q value cutoff = 0.05 (79).

TCGA GBM data analysis

The Cancer Genome Atlas (TCGA) miR expression level-3 data and metadata containing the survival information of patients with GBM were downloaded from https://gdac.broadinstitute.org/. We ranked the patients with GBM from high to low according to their miR-10b or miR-21 expression level and then labeled the top 25% of patients as the miR-higher group and the bottom 25% ones as the miR-lower group. One patient with GBM would be marked as miR-10b–higher and miR-21–higher when this patient was in both the miR-10b–higher group and miR-21–higher group, and a miR-10b plus miR-21–lower patient was in both the miR-10b–lower group and miR-21–lower group. Survival curves were performed by Kaplan-Meier analysis between the miR-higher and miR-lower group and were tested for significance using the Mantel-Cox log-rank test. A value of P < 0.05 was considered statistically significant. Between the miR-10b and miR-21–higher and miR-10b plus miR-21–lower group, hazard ratio and confidence interval were also computed using the function coxph in package survival (3.2-7).

Western blot analysis

Total protein was isolated from U87 cell pellets using 1× radioimmunoprecipitation assay (Thermo Fisher Scientific, USA) lysis buffer containing protease inhibitor. Bicinchoninic acid assay (#23225, Thermo Fisher Scientific, USA) was used to quantify the protein as per the manufacturer's instructions. A total of 35 μg of total protein was then separated on a precast 4 to 15% polyacrylamide gel using Mini-PROTEAN electrophoresis cell (Bio-Rad, USA). The separated protein samples were transferred to a polyvinylidene fluoride membrane using semidry (for VEGFA) or wet transfer (for PDGFR-β) and blocked with 5% nonfat dry milk in 1× tris-buffered saline (#1706435, Bio-Rad, USA) and 0.1% Tween 20. Primary antibodies, VEGFA [#50661, Cell Signaling Technology (CST), USA], and PDGFR-β (#3169T, CST, USA) were used at 1:250 dilution. Vinculin (#13901T, CST, USA) and β-actin (#8457S, CST, USA) were probed as reference proteins at 1:500 and 1:2000 dilution, respectively. Anti-rabbit immunoglobulin G horseradish peroxidase (HRP)–linked secondary antibody (#7074S, CST) was used at 1:2000 dilution. Blots were then incubated with a chemiluminescent HRP substrate (#WBKLS0500, Millipore, USA) and imaged using ChemiDoc imaging system (Bio-Rad, USA). The band intensities were quantified using ImageJ version 1.51.

In vivo study of sγPNA/BNP

All procedures were approved by the Yale University Institutional Animal Care and Use Committee and performed in accordance with the guidelines and policies of the Yale Animal Resource Center. Athymic nude mice [Charles River Laboratories, Crl:NU(NCr)-Foxn1^{nu}, strain 490, male, 6 to 7 weeks] were used for the animal study.

Orthotopic tumor inoculation

Animals were anesthetized using a mixture of ketamine (100 mg/kg) and xylazine (10 mg/kg) via intraperitoneal injection. Anesthetized animals were then placed in a stereotaxic frame, and the scalp was sterilized with Betadine and alcohol. To expose the coronal and sagittal sutures, a midline scalp incision was created, and a burr hole was drilled 2 mm lateral to the sagittal suture and 0.5 mm anterior to the bregma. U87 or G22 cells ($3.5 × 10^5$) in 3 μl of PBS were injected into the right stratum over 3 min using a 10-μl Hamilton syringe. The animal was left for 5 min for tissue equilibration before and after infusion. When infusion was finished, the burr hole was filled with bone wax, and the skin was stapled and cleaned. Animals were randomly assigned to multiple groups. Animals dying without waking up from surgery (after tumor inoculation or CED) were excluded.

CED of sγPNA/BNP in the tumor bearing brain

CED in tumor-bearing mice was similar to tumor inoculation by reopening the burr hole used for tumor inoculation. A microinfusion pump (World Precision Instruments) was used to infuse 8 μl of NPs at a rate of 0.5 μl/min.

Tumor retention of sγPNA/BNP

Intracranial CED of sγPNA or sγPNA/BNP was conducted 10 days after U87 tumor implantation using the same procedure as previously described. On days 0.1 (3 hours), 1, 3, 7, and 14 after CED administration, mice were euthanized, and brains were harvested and imaged using Xenogen IVIS. The fluorescence from each brain was quantified by the instrument software. Then, the isolated brains were embedded in an optimal cutting temperature (OCT) compound, cut into 15-μm frozen sections, stained with DAPI or H&E, and observed using an EVOS microscope (FL Auto 2).

Survival study in the tumor-bearing mice

Tumors grew for 6 days before the administration of treatment. Intracranial CED of sγPNA/BNP was conducted at the sγPNA dose of 0.36 mg/kg following the same surgical procedure as described. TMZ (25 mg/kg) in PBS was administered intraperitoneally on day 7. Animals were monitored daily and weighed every week. Animals were euthanized once they showed clinical symptoms of tumor progression or greater than 15% weight loss. Tumors and major organs were harvested and fixed in 4% paraformaldehyde and sectioned for histochemical analysis. Total RNA in the tumor and contralateral hemisphere was isolated using a mirVana miRNA isolation kit and analyzed by a real-time PCR detection system as previously described.

Evaluation of miR-10b and miR-21 inhibition in tumor

To assess the in vivo knockdown effect, sγPNA/BNPs were administered by CED 14 or 28 days after tumor inoculation. Two days after CED, mice were euthanized, and brains were harvested for qRT-PCR analysis. Tumor tissue was separated from the adjacent normal brain areas of isolated brains. Total RNA was extracted from tumor tissue using the mirVana miRNA isolation kit (Ambion). miR levels were quantified using the CFX Connect Real-Time PCR Detection System and CFX Manager Software (Bio-Rad) as described.

Evaluation of DEGs selected from RNA-seq

The levels of selected genes were quantified in total RNA samples extracted from in vitro and in vivo tumor samples. The cDNA was synthesized using a high-capacity cDNA reverse transcription kit (Thermo Fisher Scientific, USA). The mRNA levels of *PDGFRA*, *PDGFRB*, *VEGFA*, *ITGB8*, *ITGA10*, *ANGPT1*, *ANGPT2*, *PRKCA*,

IL-6, and *IL-24* were quantified using TaqMan gene expression assays (*PDGFRA*: Hs00998018, *PDGFRB*: Hs01019589, *VEGFA*: Hs00900055, *ITGB8*: Hs001744546, *ITGA10*: Hs01006910, *ITGA11*: Hs01012939, *ANGPT1*: Hs00559786, *ANGPT2*: Hs00171912, *PRKCA*: Hs00176973, *IL-6*: Hs00174131, and *IL-24*: Hs01114274) (Thermo Fisher Scientific, USA) and TaqMan fast advanced master mix (Thermo Fisher Scientific, USA) on the CFX Connect Real-Time PCR Detection System (Bio-Rad, USA). *GAPDH* was used as a reference, and relative fold change was calculated using the $2^{-\Delta\Delta Ct}$ method.

Toxicity study

For the evaluation of toxicity, tumor-bearing mice were administered with sγPNA/BNP via CED 14 days after tumor inoculation. After 24 hours, TMZ (25 mg/kg) was injected intraperitoneally. Forty-eight hours after CED, blood from the retro-orbital venous plexus of each mouse was collected in EDTA tubes. The whole blood was analyzed using a Sysmex XP-300 hematological analyzer (Sysmex) to obtain the complete blood count. Plasma was isolated from blood samples via centrifugation at 4500 rpm and 4°C for 10 min. Plasma samples were then analyzed by Antech Diagnostics to obtain the blood biochemistry analysis including LDH, AST, ALT, creatinine, and BUN. Major organs (heart, liver, spleen, lung, and kidney) were isolated from the survival study mice (U87 and G22 glioma model) and sectioned for H&E staining. Blinded histological analysis of the tissue was conducted by a pathologist at Yale Medical School.

Statistical analysis

Data are presented as means ± SD or SEM. Experiments were performed with at least three biological replicates, and all samples were included in the analysis. Statistical significance analysis was performed with Prism software (GraphPad) using unpaired two-sample *t* test or one-way analysis of variance (ANOVA). Log-rank (Mantel-Cox) test was used to determine statistically significant differences between the survival of animals from different treatment groups. *P* < 0.05 was used as the minimal level of significance.

Supplementary Materials

This PDF file includes:
Figs. S1 to S33
Tables S1 and S2

Other Supplementary Material for this manuscript includes the following:
Movies S1 to S4

View/request a protocol for this paper from *Bio-protocol*.

REFERENCES AND NOTES

1. R. L. Siegel, K. D. Miller, H. E. Fuchs, A. Jemal, Cancer statistics, 2022. *CA Cancer J. Clin.* **72**, 7–33 (2022).
2. A. M. Molinaro, J. W. Taylor, J. K. Wiencke, M. R. Wrensch, Genetic and molecular epidemiology of adult diffuse glioma. *Nat. Rev. Neurol.* **15**, 405–417 (2019).
3. F. G. Davis, T. R. Smith, H. R. Gittleman, Q. T. Ostrom, C. Kruchko, J. S. Barnholtz-Sloan, Glioblastoma incidence rate trends in Canada and the United States compared with England, 1995-2015. *Neuro Oncol.* **22**, 301–302 (2020).
4. J. A. Schwartzbaum, J. L. Fisher, K. D. Aldape, M. Wrensch, Epidemiology and molecular pathology of glioma. *Nat. Clin. Pract. Neurol.* **2**, 494–503 (2006).
5. R. Stupp, W. P. Mason, M. J. van den Bent, M. Weller, B. Fisher, M. J. B. Taphoorn, K. Belanger, A. A. Brandes, C. Marosi, U. Bogdahn, J. Curschmann, R. C. Janzer, S. K. Ludwin, T. Gorlia, A. Allgeier, D. Lacombe, J. G. Cairncross, E. Eisenhauer, R. O. Mirimanoff; European Organisation for Research and Treatment of Cancer Brain Tumor and Radiotherapy Groups; National Cancer Institute of Canada Clinical Trials Group, Radiotherapy plus concomitant and adjuvant temozolomide for glioblastoma. *N. Engl. J. Med.* **352**, 987–996 (2005).
6. L. He, G. J. Hannon, MicroRNAs: Small RNAs with a big role in gene regulation. *Nat. Rev. Genet.* **5**, 522–531 (2004).
7. F. J. Slack, J. B. Weidhaas, MicroRNA in cancer prognosis. *N. Engl. J. Med.* **359**, 2720–2722 (2008).
8. S. A. Ciafre, S. Galardi, A. Mangiola, M. Ferracin, C. G. Liu, G. Sabatino, M. Negrini, G. Maira, C. M. Croce, M. G. Farace, Extensive modulation of a set of microRNAs in primary glioblastoma. *Biochem. Biophys. Res. Commun.* **334**, 1351–1358 (2005).
9. R. El Fatimy, S. Subramanian, E. J. Uhlmann, A. M. Krichevsky, Genome editing reveals glioblastoma addiction to microRNA-10b. *Mol. Ther.* **25**, 368–378 (2017).
10. G. Gabriely, M. Yi, R. S. Narayan, J. M. Niers, T. Wurdinger, J. Imitola, K. L. Ligon, S. Kesari, C. Esau, R. M. Stephens, B. A. Tannous, A. M. Krichevsky, Human glioma growth is controlled by microRNA-10b. *Cancer Res.* **71**, 3563–3572 (2011).
11. G. Gabriely, T. Wurdinger, S. Kesari, C. C. Esau, J. Burchard, P. S. Linsley, A. M. Krichevsky, MicroRNA 21 promotes glioma invasion by targeting matrix metalloproteinase regulators. *Mol. Cell. Biol.* **28**, 5369–5380 (2008).
12. C. H. Yang, J. Yue, S. R. Pfeffer, M. Fan, E. Paulus, A. Hosni-Ahmed, M. Sims, S. Qayyum, A. M. Davidoff, C. R. Handorf, L. M. Pfeffer, MicroRNA-21 promotes glioblastoma tumorigenesis by down-regulating insulin-like growth factor-binding protein-3 (IGFBP3). *J. Biol. Chem.* **289**, 25079–25087 (2014).
13. F. Guessous, M. Alvarado-Velez, L. Marcinkiewicz, Y. Zhang, J. Kim, S. Heister, B. Kefas, J. Godlewski, D. Schiff, B. Purow, R. Abounader, Oncogenic effects of miR-10b in glioblastoma stem cells. *J. Neurooncol.* **112**, 153–163 (2013).
14. N. M. Teplyuk, E. J. Uhlmann, G. Gabriely, N. Volfovsky, Y. Wang, J. Teng, P. Karmali, E. Marcusson, M. Peter, A. Mohan, Y. Kraytsberg, R. Cialic, E. A. Chiocca, J. Godlewski, B. Tannous, A. M. Krichevsky, Therapeutic potential of targeting microRNA-10b in established intracranial glioblastoma: First steps toward the clinic. *EMBO Mol. Med.* **8**, 268–287 (2016).
15. I. Ben-Porath, M. W. Thomson, V. J. Carey, R. Ge, G. W. Bell, A. Regev, R. A. Weinberg, An embryonic stem cell-like gene expression signature in poorly differentiated aggressive human tumors. *Nat. Genet.* **40**, 499–507 (2008).
16. P. Sathyan, P. O. Zinn, A. L. Marisetty, B. Liu, M. M. Kamal, S. K. Singh, P. Bady, L. Lu, K. M. Wani, B. L. Veo, J. Gumin, D. H. Kassem, F. Robinson, C. Weng, V. Baladandayuthapani, D. Suki, H. Colman, K. P. Bhat, E. P. Sulman, K. Aldape, R. R. Colen, R. G. W. Verhaak, Z. Lu, G. N. Fuller, S. Huang, F. F. Lang, R. Sawaya, M. Hegi, S. Majumder, Mir-21-Sox2 axis delineates glioblastoma subtypes with prognostic impact. *J. Neurosci.* **35**, 15097–15112 (2015).
17. M. F. Corsten, R. Miranda, R. Kasmieh, A. M. Krichevsky, R. Weissleder, K. Shah, MicroRNA-21 knockdown disrupts glioma growth in vivo and displays synergistic cytotoxicity with neural precursor cell delivered S-TRAIL in human gliomas. *Cancer Res.* **67**, 8994–9000 (2007).
18. Y. E. Seo, H. W. Suh, R. Bahal, A. Josowitz, J. Zhang, E. Song, J. Cui, S. Noorbakhsh, C. Jackson, T. Bu, A. Piotrowski-Daspit, R. Bindra, W. M. Saltzman, Nanoparticle-mediated intratumoral inhibition of miR-21 for improved survival in glioblastoma. *Biomaterials* **201**, 87–98 (2019).
19. L. Shi, J. Chen, J. Yang, T. Pan, S. Zhang, Z. Wang, MiR-21 protected human glioblastoma U87MG cells from chemotherapeutic drug temozolomide induced apoptosis by decreasing Bax/Bcl-2 ratio and caspase-3 activity. *Brain Res.* **1352**, 255–264 (2010).
20. Y. Ren, X. Zhou, M. Mei, X. B. Yuan, L. Han, G. X. Wang, Z. F. Jia, P. Xu, P. Y. Pu, C. S. Kang, MicroRNA-21 inhibitor sensitizes human glioblastoma cells U251 (PTEN-mutant) and LN229 (PTEN-wild type) to taxol. *BMC Cancer* **10**, 27 (2010).
21. J. S. Ananta, R. Paulmurugan, T. F. Massoud, Tailored nanoparticle codelivery of antimiR-21 and antimiR-10b augments glioblastoma cell kill by temozolomide: Toward a "personalized" anti-microRNA therapy. *Mol. Pharm.* **13**, 3164–3175 (2016).
22. C. G. Dong, W. K. K. Wu, S. Y. Feng, X. J. Wang, J. F. Shao, J. Qiao, Co-inhibition of microRNA-10b and microRNA-21 exerts synergistic inhibition on the proliferation and invasion of human glioma cells. *Int. J. Oncol.* **41**, 1005–1012 (2012).
23. M. Malhotra, T. V. Sekar, J. S. Ananta, R. Devulapally, R. Afjei, H. A. Babikir, R. Paulmurugan, T. F. Massoud, Targeted nanoparticle delivery of therapeutic antisense microRNAs presensitizes glioblastoma cells to lower effective doses of temozolomide in vitro and in a mouse model. *Oncotarget* **9**, 21478–21494 (2018).
24. P. E. Nielsen, M. Egholm, R. H. Berg, O. Buchardt, Sequence-selective recognition of DNA by strand displacement with a thymine-substituted polyamide. *Science* **254**, 1497–1500 (1991).
25. V. V. Demidov, V. N. Potaman, M. D. Frank-Kamenetskii, M. Egholm, O. Buchard, S. H. Sönnichsen, P. E. Nielsen, Stability of peptide nucleic acids in human serum and cellular extracts. *Biochem. Pharmacol.* **48**, 1310–1313 (1994).

26. M. Egholm, O. Buchardt, L. Christensen, C. Behrens, S. M. Freier, D. A. Driver, R. H. Berg, S. K. Kim, B. Norden, P. E. Nielsen, PNA hybridizes to complementary oligonucleotides obeying the Watson-Crick hydrogen-bonding rules. *Nature* **365**, 566–568 (1993).

27. I. A. Babar, C. J. Cheng, C. J. Booth, X. Liang, J. B. Weidhaas, W. M. Saltzman, F. J. Slack, Nanoparticle-based therapy in an in vivo microRNA-155 (miR-155)-dependent mouse model of lymphoma. *Proc. Natl. Acad. Sci. U.S.A.* **109**, E1695–E1704 (2012).

28. C. J. Cheng, R. Bahal, I. A. Babar, Z. Pincus, F. Barrera, C. Liu, A. Svoronos, D. T. Braddock, P. M. Glazer, D. M. Engelman, W. M. Saltzman, F. J. Slack, MicroRNA silencing for cancer therapy targeted to the tumour microenvironment. *Nature* **518**, 107–110 (2015).

29. D. P. Bartel, MicroRNAs: Target recognition and regulatory functions. *Cell* **136**, 215–233 (2009).

30. S. Obad, C. O. dos Santos, A. Petri, M. Heidenblad, O. Broom, C. Ruse, C. Fu, M. Lindow, J. Stenvang, E. M. Straarup, H. F. Hansen, T. Koch, D. Pappin, G. J. Hannon, S. Kauppinen, Silencing of microRNA families by seed-targeting tiny LNAs. *Nat. Genet.* **43**, 371–378 (2011).

31. A. Dragulescu-Andrasi, S. Rapireddy, B. M. Frezza, C. Gayathri, R. R. Gil, D. H. Ly, A simple gamma-backbone modification preorganizes peptide nucleic acid into a helical structure. *J. Am. Chem. Soc.* **128**, 10258–10267 (2006).

32. B. G. Garchow, O. Bartulos Encinas, Y. T. Leung, P. Y. Tsao, R. A. Eisenberg, R. Caricchio, S. Obad, A. Petri, S. Kauppinen, M. Kiriakidou, Silencing of microRNA-21 in vivo ameliorates autoimmune splenomegaly in lupus mice. *EMBO Mol. Med.* **3**, 605–615 (2011).

33. V. Rottiers, S. Obad, A. Petri, R. McGarrah, M. W. Lindholm, J. C. Black, S. Sinha, R. J. Goody, M. S. Lawrence, A. S. deLemos, H. F. Hansen, S. Whittaker, S. Henry, R. Brookes, S. H. Najafi-Shoushtari, R. T. Chung, J. R. Whetstine, R. E. Gerszten, S. Kauppinen, A. M. Näär, Pharmacological inhibition of a microRNA family in nonhuman primates by a seed-targeting 8-mer antimiR. *Sci. Transl. Med.* **5**, 212ra162 (2013).

34. Y. E. Seo, T. Bu, W. M. Saltzman, Nanomaterials for convection-enhanced delivery of agents to treat brain tumors. *Curr. Opin. Biomed. Eng.* **4**, 1–12 (2017).

35. Y. Deng, J. K. Saucier-Sawyer, C. J. Hoimes, J. Zhang, Y. E. Seo, J. W. Andrejecsk, W. M. Saltzman, The effect of hyperbranched polyglycerol coatings on drug delivery using degradable polymer nanoparticles. *Biomaterials* **35**, 6595–6602 (2014).

36. Y. Deng, A. Ediriwickrema, F. Yang, J. Lewis, M. Girardi, W. M. Saltzman, A sunblock based on bioadhesive nanoparticles. *Nat. Mater.* **14**, 1278–1285 (2015).

37. H. W. Suh, J. Lewis, L. Fong, J. Y. Ramseier, K. Carlson, Z. H. Peng, E. S. Yin, W. M. Saltzman, M. Girardi, Biodegradable bioadhesive nanoparticle incorporation of broad-spectrum organic sunscreen agents. *Bioeng. Transl. Med.* **4**, 129–140 (2019).

38. E. Song, A. Gaudin, A. R. King, Y. E. Seo, H. W. Suh, Y. Deng, J. Cui, G. T. Tietjen, A. Huttner, W. M. Saltzman, Surface chemistry governs cellular tropism of nanoparticles in the brain. *Nat. Commun.* **8**, 15322 (2017).

39. L. Christensen, R. Fitzpatrick, B. Gildea, K. H. Petersen, H. F. Hansen, T. Koch, M. Egholm, O. Buchardt, P. E. Nielsen, J. Coull, R. H. Berg, Solid-phase synthesis of peptide nucleic acids. *J. Pept. Sci.* **1**, 175–183 (1995).

40. S. Malik, J. Lim, F. J. Slack, D. T. Braddock, R. Bahal, Next generation miRNA inhibition using short anti-seed PNAs encapsulated in PLGA nanoparticles. *J. Control. Release* **327**, 406–419 (2020).

41. J. K. Hu, H. W. Suh, M. Qureshi, J. M. Lewis, S. Yaqoob, Z. M. Moscato, S. Griff, A. K. Lee, E. S. Yin, W. M. Saltzman, M. Girardi, Nonsurgical treatment of skin cancer with local delivery of bioadhesive nanoparticles. *Proc. Natl. Acad. Sci. U.S.A.* **118**, (2021).

42. Y.-R. Lee, M. Chen, P. P. Pandolfi, The functions and regulation of the PTEN tumour suppressor: New modes and prospects. *Nat. Rev. Mol. Cell Biol.* **19**, 547–562 (2018).

43. F. Meng, R. Henson, H. Wehbe-Janek, K. Ghoshal, S. T. Jacob, T. Patel, MicroRNA-21 regulates expression of the PTEN tumor suppressor gene in human hepatocellular cancer. *Gastroenterology* **133**, 647–658 (2007).

44. M. Mizoguchi, Y. Guan, K. Yoshimoto, N. Hata, T. Amano, A. Nakamizo, T. Sasaki, Clinical implications of microRNAs in human glioblastoma. *Front. Oncol.* **3**, 19 (2013).

45. H. A. Hamed, A. Yacoub, M. A. Park, P. J. Eulitt, R. Dash, D. Sarkar, I. P. Dmitriev, M. S. Lesniak, K. Shah, S. Grant, D. T. Curiel, P. B. Fisher, P. Dent, Inhibition of multiple protective signaling pathways and Ad.5/3 delivery enhances mda-7/IL-24 therapy of malignant glioma. *Mol. Ther.* **18**, 1130–1142 (2010).

46. T. Lin, D. Wang, J. Chen, Z. Zhang, Y. Zhao, Z. Wu, Y. Wang, IL-24 inhibits the malignancy of human glioblastoma cells via destabilization of Zeb1. *Biol. Chem.* **402**, 839–848 (2021).

47. B. L. Carlson, J. L. Pokorny, M. A. Schroeder, J. N. Sarkaria, Establishment, maintenance and in vitro and in vivo applications of primary human glioblastoma multiforme (GBM) xenograft models for translational biology studies and drug discovery. *Curr. Protoc. Pharmacol.* **Chapter 14**, Unit 14.16, (2011).

48. Q. T. Ostrom, H. Gittleman, J. Fulop, M. Liu, R. Blanda, C. Kromer, Y. Wolinsky, C. Kruchko, J. S. Barnholtz-Sloan, CBTRUS statistical report: Primary brain and central nervous system tumors diagnosed in the United States in 2008–2012. *Neuro Oncol.* **17**, iv1–iv62 (2015).

49. B. M. Alexander, T. F. Cloughesy, Adult glioblastoma. *J. Clin. Oncol.* **35**, 2402–2409 (2017).

50. J. Wang, E. Cazzato, E. Ladewig, V. Frattini, D. I. S. Rosenbloom, S. Zairis, F. Abate, Z. Liu, O. Elliott, Y.-J. Shin, J.-K. Lee, I.-H. Lee, W.-Y. Park, M. Eoli, A. J. Blumberg, A. Lasorella, D.-H. Nam, G. Finocchiaro, A. Iavarone, R. Rabadan, Clonal evolution of glioblastoma under therapy. *Nat. Genet.* **48**, 768–776 (2016).

51. M. Lim, Y. Xia, C. Bettegowda, M. Weller, Current state of immunotherapy for glioblastoma. *Nat. Rev. Clin. Oncol.* **15**, 422–442 (2018).

52. C. W. Brennan, R. G. W. Verhaak, A. McKenna, B. Campos, H. Noushmehr, S. R. Salama, S. Zheng, D. Chakravarty, J. Z. Sanborn, S. H. Berman, R. Beroukhim, B. Bernard, C.-J. Wu, G. Genovese, I. Shmulevich, J. Barnholtz-Sloan, L. Zou, R. Vegesna, S. A. Shukla, G. Ciriello, W. K. Yung, W. Zhang, C. Sougnez, T. Mikkelsen, K. Aldape, D. D. Bigner, E. G. Van Meir, M. Prados, A. Sloan, K. L. Black, J. Eschbacher, G. Finocchiaro, W. Friedman, D. W. Andrews, A. Guha, M. Iacocca, B. P. O'Neill, G. Foltz, J. Myers, D. J. Weisenberger, R. Penny, R. Kucherlapati, C. M. Perou, D. N. Hayes, R. Gibbs, M. Marra, G. B. Mills, E. Lander, P. Spellman, R. Wilson, C. Sander, J. Weinstein, M. Meyerson, S. Gabriel, P. W. Laird, D. Haussler, G. Getz, L. Chin; TCGA Research Network, The somatic genomic landscape of glioblastoma. *Cell* **155**, 462–477 (2013).

53. M. Petersen, J. Wengel, LNA: A versatile tool for therapeutics and genomics. *Trends Biotechnol.* **21**, 74–81 (2003).

54. J. A. Chan, A. M. Krichevsky, K. S. Kosik, MicroRNA-21 is an antiapoptotic factor in human glioblastoma cells. *Cancer Res.* **65**, 6029–6033 (2005).

55. G. Zhang, L. Q. Jin, L. Hu, W. Rodemer, M. E. Selzer, Antisense morpholino oligonucleotides reduce neurofilament synthesis and inhibit axon regeneration in lamprey reticulospinal neurons. *PLOS ONE* **10**, e0137670 (2015).

56. L. L. Muldoon, C. Soussain, K. Jahnke, C. Johanson, T. Siegal, Q. R. Smith, W. A. Hall, K. Hynynen, P. D. Senter, D. M. Peereboom, E. A. Neuwelt, Chemotherapy delivery issues in central nervous system malignancy: A reality check. *J. Clin. Oncol.* **25**, 2295–2305 (2007).

57. I. T. Papademetriou, T. Porter, Promising approaches to circumvent the blood-brain barrier: Progress, pitfalls and clinical prospects in brain cancer. *Ther. Deliv.* **6**, 989–1016 (2015).

58. R. H. Bobo, D. W. Laske, A. Akbasak, P. F. Morrison, R. L. Dedrick, E. H. Oldfield, Convection-enhanced delivery of macromolecules in the brain. *Proc. Natl. Acad. Sci. U.S.A.* **91**, 2076–2080 (1994).

59. M. A. Vogelbaum, M. K. Aghi, Convection-enhanced delivery for the treatment of glioblastoma. *Neuro Oncol.* **17** (Suppl. 2), ii3–ii8 (2015).

60. J. N. Bruce, R. L. Fine, P. Canoll, J. Yun, B. C. Kennedy, S. S. Rosenfeld, S. A. Sands, K. Surapaneni, R. Lai, C. L. Yanes, E. Bagiella, R. L. DeLaPaz, Regression of recurrent malignant gliomas with convection-enhanced delivery of topotecan. *Neurosurgery* **69**, 1272–1279 (2011).

61. U. Bogdahn, P. Hau, G. Stockhammer, N. K. Venkataramana, A. K. Mahapatra, A. Suri, A. Balasubramaniam, S. Nair, V. Oliushine, V. Parfenov, I. Poverennova, M. Zaaroor, P. Jachimczak, S. Ludwig, S. Schmaus, H. Heinrichs, K.-H. Schlingensiepen; Trabedersen Glioma Study Group, Targeted therapy for high-grade glioma with the TGF-2 inhibitor trabedersen: Results of a randomized and controlled phase IIb study. *Neuro Oncol.* **13**, 132–142 (2011).

62. J. Voges, R. Reszka, A. Gossmann, C. Dittmar, R. Richter, G. Garlip, L. Kracht, H. H. Coenen, V. Sturm, K. Wienhard, W. D. Heiss, A. H. Jacobs, Imaging-guided convection-enhanced delivery and gene therapy of glioblastoma. *Ann. Neurol.* **54**, 479–487 (2003).

63. G. M. Bernal, M. J. LaRiviere, N. Mansour, P. Pytel, K. E. Cahill, D. J. Voce, S. Kang, R. Spretz, U. Welp, S. E. Noriega, L. Nunez, G. F. Larsen, R. R. Weichselbaum, B. Yamini, Convection-enhanced delivery and in vivo imaging of polymeric nanoparticles for the treatment of malignant glioma. *Nanomedicine* **10**, 149–157 (2014).

64. N. U. Barua, M. Woolley, A. S. Bienemann, D. Johnson, M. J. Wyatt, C. Irving, O. Lewis, E. Castrique, S. S. Gill, Convection-enhanced delivery of AAV2 in white matter—A novel method for gene delivery to cerebral cortex. *J. Neurosci. Methods* **220**, 1–8 (2013).

65. E. Allard, C. Passirani, J. P. Benoit, Convection-enhanced delivery of nanocarriers for the treatment of brain tumors. *Biomaterials* **30**, 2302–2318 (2009).

66. A. M. Mehta, A. M. Sonabend, J. N. Bruce, Convection-enhanced delivery. *Neurotherapeutics* **14**, 358–371 (2017).

67. J. H. Sampson, G. Archer, C. Pedain, E. Wembacher-Schröder, M. Westphal, S. Kunwar, M. A. Vogelbaum, A. Coan, J. E. Herndon, R. Raghavan, M. L. Brady, D. A. Reardon, A. H. Friedman, H. S. Friedman, M. I. Rodríguez-Ponce, S. M. Chang, S. Mittermeyer, D. Croteau, R. K. Puri; PRECISE Trial Investigators, Poor drug distribution as a possible explanation for the results of the PRECISE trial. *J. Neurosurg.* **113**, 301–309 (2010).

68. J. H. Kang, A. Desjardins, Convection-enhanced delivery for high-grade glioma. *Neuro-oncol. Pract.* **9**, 24–34 (2022).

69. E. F. Spinazzi, M. G. Argenziano, P. S. Upadhyayula, M. A. Banu, J. A. Neira, D. M. O. Higgins, P. B. Wu, B. Pereira, A. Mahajan, N. Humala, O. Al-Dalahmah, W. Zhao, A. V. Save, B. J. A. Gill, D. M. Boyett, T. Marie, J. L. Furnari, T. D. Sudhakar, S. A. Stopka, M. S. Regan, V. Catania, L. Good, S. Zacharoulis, M. Behl, P. Petridis, S. Jambawalikar, A. Mintz, A. Lignelli, N. Y. R. Agar, P. A. Sims, M. R. Welch, A. B. Lassman, F. M. Iwamoto, R. S. D'Amico, J. Grinband, P. Canoll, J. N. Bruce, Chronic convection-enhanced delivery of topotecan for patients with

recurrent glioblastoma: A first-in-patient, single-centre, single-arm, phase 1b trial. *Lancet Oncol.* **23**, 1409–1418 (2022).

70. J. S. Young, M. K. Aghi, Chronic convection-enhanced intratumoural delivery of chemotherapy for glioblastoma. *Lancet Oncol.* **23**, 1347–1348 (2022).

71. J. K. Saucier-Sawyer, Y. E. Seo, A. Gaudin, E. Quijano, E. Song, A. J. Sawyer, Y. Deng, A. Huttner, W. M. Saltzman, Distribution of polymer nanoparticles by convection-enhanced delivery to brain tumors. *J. Control. Release* **232**, 103–112 (2016).

72. H. Gibori, S. Eliyahu, A. Krivitsky, D. Ben-Shushan, Y. Epshtein, G. Tiram, R. Blau, P. Ofek, J. S. Lee, E. Ruppin, L. Landsman, I. Barshack, T. Golan, E. Merquiol, G. Blum, R. Satchi-Fainaro, Amphiphilic nanocarrier-induced modulation of PLK1 and miR-34a leads to improved therapeutic response in pancreatic cancer. *Nat. Commun.* **9**, 16 (2018).

73. E. Jonsson, H. Fridborg, P. Nygren, R. Larsson, Synergistic interactions of combinations of topotecan with standard drugs in primary cultures of human tumor cells from patients. *Eur. J. Clin. Pharmacol.* **54**, 509–514 (1998).

74. P. P. Wang, J. Frazier, H. Brem, Local drug delivery to the brain. *Adv. Drug Deliv. Rev.* **54**, 987–1013 (2002).

75. A. J. Sawyer, J. M. Piepmeier, W. M. Saltzman, Cancer issue: New methods for direct delivery of chemotherapy for treating brain tumors. *Yale J. Biol. Med.* **79**, 141–152 (2006).

76. A. F. Haddad, J. S. Young, D. Amara, M. S. Berger, D. R. Raleigh, M. K. Aghi, N. A. Butowski, Mouse models of glioblastoma for the evaluation of novel therapeutic strategies. *Neurooncol. Adv.* **3**, vdab100 (2021).

77. B. Sahu, I. Sacui, S. Rapireddy, K. J. Zanotti, R. Bahal, B. A. Armitage, D. H. Ly, Synthesis and characterization of conformationally preorganized, (R)-diethylene glycol-containing γ-peptide nucleic acids with superior hybridization properties and water solubility. *J. Organomet. Chem.* **76**, 5614–5627 (2011).

78. M. I. Love, W. Huber, S. Anders, Moderated estimation of fold change and dispersion for RNA-seq data with DESeq2. *Genome Biol.* **15**, 550 (2014).

79. G. Yu, L.-G. Wang, Y. Han, Q.-Y. He, clusterProfiler: An R package for comparing biological themes among gene clusters. *OMICS* **16**, 284–287 (2012).